Nonmodal Stability Theory

Peter J. Schmid

Laboratoire d'Hydrodynamique (LadHyX), CNRS-École Polytechnique,
F-91128 Palaiseau, France; email: peter@ladhyx.polytechnique.fr

Annu. Rev. Fluid Mech. 2007. 39:129–62

The *Annual Review of Fluid Mechanics* is online at fluid.annualreviews.org

This article's doi:
10.1146/annurev.fluid.38.050304.092139

0066-4189/07/0115-0129$20.00

Key Words

transient growth, transition, non-normal operators, pseudospectra, transfer function, impulse response

Abstract

Hydrodynamic stability theory has recently seen a great deal of development. After being dominated by modal (eigenvalue) analysis for many decades, a different perspective has emerged that allows the quantitative description of short-term disturbance behavior. A general formulation based on the linear initial-value problem, thus circumventing the normal-mode approach, yields an efficient framework for stability calculations that is easily extendable to incorporate time-dependent flows, spatially varying configurations, stochastic influences, nonlinear effects, and flows in complex geometries.

1. INTRODUCTION

The emergence of spatial patterns, the observation of consistent temporal behavior, and the interplay of coherent structures in fluid flows have provided the basic motivation for the development of hydrodynamic stability theory. As evidenced in the early drawings of Leonardo da Vinci, which illustrate the intricate details of vortex patterns forming in the wake of rocks in a stream, the question of why, when, and how fluid motion deviates from its ordered state to exhibit more complex behavior has fascinated scientists and laymen alike.

1.1. Historical Perspective

As the first controlled scientific experiment, the setup of Reynolds (1883) is often acknowledged, and frequently cited, as the beginning of modern hydrodynamic stability theory, introducing the now familiar Reynolds number *Re* as a critical nondimensional parameter that distinguishes stable from unstable flows. In the decades following Reynolds, hydrodynamic stability theory evolved and matured significantly, and important accomplishments were achieved. These early accomplishments predated the advent of computational means and thus relied on simplifying assumptions and sophisticated asymptotic techniques (Drazin & Reid 1981). Some of the now classical results in stability theory, obtained throughout the past century, include the formulation of the viscous stability problem for parallel shear flows (Orr 1907, Sommerfeld 1908), which had to await its accurate numerical solution for plane Poiseuille flow many years later (Orszag 1971), bounds on maximum energy growth (Joseph 1976), the theoretical prediction (Schlichting 1933, Tollmien 1929) and experimental observation of Tollmien-Schlichting waves (Klebanoff et al. 1962), their secondary instability (Herbert 1988, Orszag & Patera 1983), the identification of instability waves in compressible boundary layers (Mack 1963), the discovery and description of Taylor rolls (Taylor 1923), a mathematical framework for spatially growing disturbances (Gaster 1965), the derivation of rigorous criteria for absolutely growing disturbances (Huerre & Monkewitz 1990), the discovery of elliptical instabilities (Bayly 1986, Pierrehumbert 1986), the description of complex flow situations by the parabolized stability equations (Bertolotti et al. 1992, Chang & Malik 1994), and many more.

Despite these remarkable accomplishments, many questions were left unanswered, including the discrepancy between the computed critical Reynolds number and the observed transitional Reynolds number in many wall-bounded shear flows, the interplay between linear energy amplification and nonlinear energy conservation in the subcritical regime, the nonexistence of finite critical Reynolds numbers for pipe or plane Couette flow, and a frequent failure to observe theoretically predicted structures in unforced experiments.

A common simplification in many stability calculations has been the assumption of an exponential time dependence, also referred to as the normal-mode approach. This ansatz allows the transformation of the linear initial-value problem into a corresponding eigenvalue problem. The computed eigenvalues are then investigated

as to their exponential growth rate, and the basic flow is subsequently labeled unstable if an eigenvalue is found in the unstable complex half-plane. The limiting nature of this modal approach was recognized and linked to the above-mentioned shortcomings in the late 1980s, and a novel way of describing fluid stability has quickly emerged (see, e.g., Boberg & Brosa 1988, Butler & Farrell 1992, Gustavsson 1991, Reddy et al. 1993, Reddy & Henningson 1993, Schmid & Henningson 2001, Trefethen et al. 1993). This new approach—the subject of this review—has enjoyed substantial success in furthering a more complete understanding of instabilities and in providing the missing mechanisms of transition in a variety of wall-bounded shear flows.

1.2. Short-Term Stability Analysis

In general, linear stability theory is concerned with a quantitative description of flow behavior involving infinitesimal disturbances superimposed on a base flow. Traditionally, the description of this behavior was inferred from the spectrum or eigenvalues of the governing linear operator. However, for most wall-bounded shear flows the spectrum is a poor proxy for the disturbance behavior as it only describes the asymptotic ($t \to \infty$) fate of the perturbation and fails to capture short-term characteristics (Schmid & Henningson 2001). The many decades-long concentration on eigenvalues in hydrodynamic stability theory has accordingly resulted in a disregard for short-time perturbation dynamics and its consequences on scale selection and transition scenarios. As an example, the maximum growth rate for plane Poiseuille flow is about 0.04 (nondimensionalized by the half-channel height and the centerline velocity) for two-dimensional streamwise perturbations. At this growth rate, it would take the least stable mode about 57 time units to grow by one order of magnitude. Experimental observations report instabilities and transition scenarios on a substantially shorter timescale. In fact, the time-asymptotic fate, as well as the shape of the least stable mode, may be irrelevant to the overall perturbation dynamics, as this limit may never, or only under artificial conditions, be reached.

To accurately describe the disturbance behavior for all times, it appears necessary to introduce a finite-time horizon over which an instability is observed. In addition, a general, unbiased analysis should determine the most amplified perturbations and describe their evolution in time. Finite-time stability analysis markedly deviates from the traditional Lyapunov stability concept (Khalil 2002), and it is not surprising that the disturbance that grows the most over a short timescale differs significantly from the least stable mode. By limiting the time horizon, new concepts and techniques have to be employed to quantitatively describe the perturbation dynamics (Schmid & Henningson 2001); at the same time, these new tools reveal a very different and remarkably rich picture of linear disturbance behavior.

Stability is redefined in a broader sense as the response behavior of the governing equations to general (deterministic or random) input variables, whether they be in the form of initial conditions, an external disturbance environment, internal uncertainties, or geometric constraints (**Figure 1**). No a priori selection of a time horizon or perturbation shape is made.

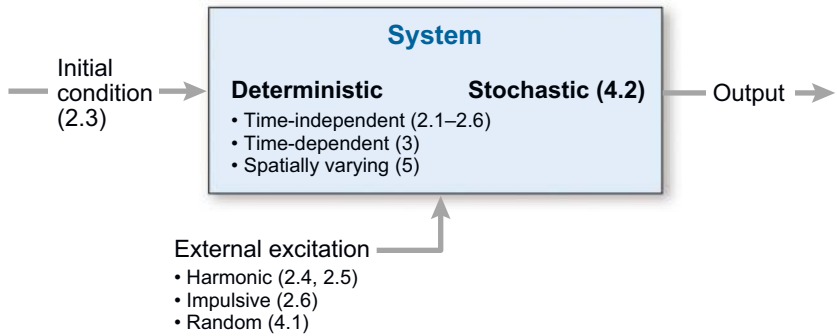

Figure 1

Sketch of a system subject to external and internal perturbations. The system is governed by a deterministic or stochastic operator and, for stability calculations, acts as a mapping of initial conditions or external excitations onto output variables. The numbers in parentheses refer to section numbers in this review.

A concise introduction to the central techniques of nonmodal stability theory is given. This review begins with classical plane Poiseuille flow, then adds periodic and aperiodic time dependence, and assesses the influence of stochastic forcing stemming from both external and internal sources; extensions to treat complex geometries, remarks on nonlinear problems, and a speculative outlook for future developments conclude this review.

2. DESCRIBING DISTURBANCE BEHAVIOR: THE NONMODAL APPROACH

Two general approaches can be distinguished: the response to initial conditions, and the response to external forcing. The first approach is central to hydrodynamic stability theory, whereas the second ventures into the closely related field of receptivity analysis (Choudhari 1993, Crouch 1994, Goldstein & Hultgren 1989, Morkoovin 1960). The two distinct viewpoints are treated within the same framework.

2.1. Governing Equations and General Solutions

We start by concentrating on the linearized incompressible Navier-Stokes equations describing the evolution of infinitesimal perturbations in a simple three-dimensional geometry with two homogeneous and one inhomogeneous directions. The concepts underlying the nonmodal approach to stability theory can readily be developed and illustrated in this simple flow situation. In subsequent sections additional features and effects, such as unsteadiness, spatial inhomogeneity, etc. are treated; as a starting point, however, the flow between parallel plates, i.e., plane Poiseuille flow, will suffice to demonstrate the nonmodal approach.

The set of governing equations is conveniently written in the form

$$\frac{\partial}{\partial t}\begin{pmatrix} v \\ \eta \end{pmatrix} = \underbrace{\begin{pmatrix} \mathbf{L}_{OS} & 0 \\ \mathbf{L}_C & \mathbf{L}_{SQ} \end{pmatrix}}_{\mathbf{A}} \begin{pmatrix} v \\ \eta \end{pmatrix} + \underbrace{\begin{pmatrix} i\alpha\mathbf{M}^{-1}\mathbf{D} & \mathbf{M}^{-1}k^2 & i\beta\mathbf{M}^{-1}\mathbf{D} \\ i\beta & 0 & -i\alpha \end{pmatrix}}_{\mathbf{B}} \begin{pmatrix} u_{in}(t) \\ v_{in}(t) \\ w_{in}(t) \end{pmatrix}, \quad (2.1a)$$

$$\begin{pmatrix} u_{out} \\ v_{out} \\ w_{out} \end{pmatrix} = \underbrace{\begin{pmatrix} \frac{i\alpha}{k^2}\mathbf{D} & -\frac{i\beta}{k^2} \\ 1 & 0 \\ \frac{i\beta}{k^2}\mathbf{D} & \frac{i\alpha}{k^2} \end{pmatrix}}_{\mathbf{C}} \begin{pmatrix} v \\ \eta \end{pmatrix}, \qquad \begin{pmatrix} u \\ v \\ w \end{pmatrix}\Big|_{t=0} = \begin{pmatrix} u_0 \\ v_0 \\ w_0 \end{pmatrix}, \quad (2.1b)$$

where $\mathbf{L}_{OS}, \mathbf{L}_{SQ}$, and $\mathbf{L}_C$ are the familiar Orr-Sommerfeld, Squire, and coupling operators, respectively, v and η stand for the wall-normal velocity and vorticity, and u, w describe the velocity components in the streamwise and spanwise coordinate directions. A Fourier transform in the two homogeneous (x, z) directions has been assumed, with α denoting the streamwise wave number, β denoting the spanwise wave number, and $k = \sqrt{\alpha^2 + \beta^2}$ as the modulus of the wave vector. The nondimensional form of the base profile is given as $U(y) = 1-y^2$, and the Reynolds number Re is based on the centerline velocity and the half-channel height. In the above formulation, it is assumed that the wall-normal y-direction has been appropriately discretized, yielding the differentiation matrix denoted by $\mathbf{D}$. The matrix $\mathbf{M}$ is given as $k^2 - \mathbf{D}^2$. Besides the governing parameters, the evolution of infinitesimal disturbances is influenced by the initial conditions (u_0, v_0, w_0) as well as by the external (time-dependent) forcing functions (u_{in}, v_{in}, w_{in}). The output variables are given by $(u_{out}, v_{out}, w_{out})$. Both the initial conditions and external forcing functions have a specified shape in the wall-normal direction.

The solution to this forced initial-value problem is given in general form by

$$\begin{pmatrix} u_{out} \\ v_{out} \\ w_{out} \end{pmatrix} = \mathbf{C}\exp(t\mathbf{A})\mathbf{B}\begin{pmatrix} u_0 \\ v_0 \\ w_0 \end{pmatrix} + \mathbf{C}\int_0^t \exp((t-\tau)\mathbf{A})\mathbf{B}\begin{pmatrix} u_{in}(\tau) \\ v_{in}(\tau) \\ w_{in}(\tau) \end{pmatrix} d\tau. \quad (2.2)$$

This general solution clearly distinguishes the response to initial conditions and the response to external forcing. Expression 2.2 represents the general dynamics of the system (Expression 2.1) and thus completely describes the behavior of disturbances governed by Expression 2.1. No approximations regarding the shape of disturbances or their temporal behavior have been introduced so far.

2.2. Choice of Measure

In any hydrodynamic stability analysis of a given flow one must first decide on an appropriate measure of the disturbance size. As seen below, the necessity for this exercise does not stem only from physical considerations, as the mathematical framework into which the analysis is cast also requires a measure of size (norm) as well as a measure of

angle (scalar product). Physically motivated measures are, of course, greatly preferred as they suggest realizability and observability for numerical simulations and physical experiments. This restriction, however, still leaves many options, and, in general, a clear and obvious choice is seldom available. For simple incompressible flows the kinetic energy of the perturbation is a convenient and defensible choice. But as soon as additional effects (free surfaces or compressibility, for example) or slightly more complex base flows (e.g., swept attachment-line flow) come into play, the definition of a scalar product and associated norm has to be reassessed. Despite some shortcomings, physically motivated disturbance measures are still the best choice; it is important, however, to interpret the results of the stability analysis with this choice in mind.

The weight necessary to convert an energy measure to the more standard Eulerian L_2 norm is not explicitly specified. Expressing the energy E of a disturbance given by the state vector $\mathbf{q} = (u, v, w)^T$ as $E = \mathbf{q}^H \mathbf{W} \mathbf{q}$ with $\mathbf{W}$ containing the appropriate integration weights, we can easily derive an energy-based norm for the state vector as $\|\mathbf{q}\|_E = \|\mathbf{F}\mathbf{q}\|_2$ and for matrices as $\|\mathbf{A}\|_E = \|\mathbf{F}\mathbf{A}\mathbf{F}^{-1}\|_2$, with $\mathbf{F}$ arising from a Cholesky decomposition of $\mathbf{W} = \mathbf{F}^H\mathbf{F}$ (Reddy et al. 1993, Schmid & Henningson 2001, Trefethen & Embree 2005). In what follows, the subscript $_E$ is omitted.

2.3. Response to Initial Conditions

The most common approach to hydrodynamic stability theory is dominated by the quest for the most dangerous initial condition that results in the maximum amplification of its kinetic energy, or, in other words, the maximum response to varying initial conditions. We are thus interested in the maximum amplification $G(t)$ of initial energy over a specified time interval, which, based on Equation 2.2, can be formulated as

$$G(t) = \max_{\mathbf{q}_0} \frac{\|\mathbf{q}(t)\|^2}{\|\mathbf{q}_0\|^2} = \max_{\mathbf{q}_0} \frac{\|\mathbf{C}\exp(t\mathbf{A})\mathbf{B}\mathbf{q}_0\|^2}{\|\mathbf{q}_0\|^2} = \|\mathbf{C}\exp(t\mathbf{A})\mathbf{B}\|^2. \qquad (2.3)$$

Note that the quantity $G(t)$ includes an optimization over all initial conditions and that for each choice of t a different initial condition may yield the maximum possible energy amplification.

Traditionally, the amplification of disturbances has been characterized in terms of the least stable mode of $\mathbf{A}$. This specific perturbation is often thought to dominate the dynamics governed by Equation 2.1. Concentrating on only the least stable mode is equivalent to replacing the norm of the operator $G(t) = \|\mathbf{C}\exp(t\mathbf{A})\mathbf{B}\|^2$ by $g(t) = \exp(2t\lambda_r)$ with λ_r as the real part of the least stable eigenvalue of $\mathbf{A}$. Using the eigenvalue decomposition of $\mathbf{A}$, i.e., $\mathbf{A} = \mathbf{V}\Lambda\mathbf{V}^{-1}$, it should become obvious that no information about the eigenfunctions of $\mathbf{A}$, contained in $\mathbf{V}$, is considered when only the least stable mode is taken as a representation of the operator exponential

$$G(t) = \|\mathbf{C}\exp(t\mathbf{A})\mathbf{B}\|^2 = \|\mathbf{C}\mathbf{V}\underbrace{\exp(t\Lambda)}_{\substack{\text{spectral}\\ \text{analysis}}}\mathbf{V}^{-1}\mathbf{B}\|^2. \qquad (2.4)$$

Spectral analysis thus only concentrates on parts of the full evolution operator. Only for unitary matrices $\mathbf{V}$, i.e., for a set of orthogonal eigenfunctions, does the real part

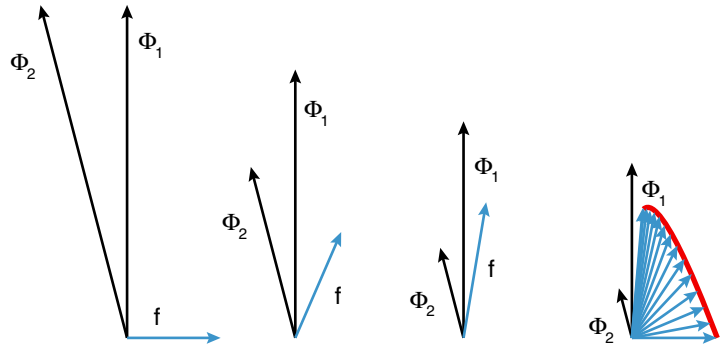

Figure 2

Vector example of transient growth. Starting on the left, the vector **f** is defined as the difference between the nearly collinear vectors Φ_1 and Φ_2. During iteration (proceeding to the right of the figure), the vector Φ_1 decreases in length by 20% whereas vector Φ_2 shrinks by 50%. The vector **f** gradually turns into the direction of Φ_1 (sketch on the right), but increases substantially in length, before decaying to zero. Thus, the superposition of decaying nonorthogonal eigenfunctions can produce, in the short term, growth in the norm of a perturbation. The same scenario with orthogonal vectors Φ_1 and Φ_2 would have resulted in monotonic decay of the norm of **f**.

of the least stable eigenvalue accurately describe the norm of the matrix exponential for all time. In this case, the similarity transformation has no effect on the value of the norm.

Matrix operators with a set of orthogonal eigenvectors are referred to as normal (Trefethen 1997, Trefethen & Embree 2005). Unfortunately, many operators in fluid dynamics and, specifically, the above matrix operator **A** are non-normal and thus have a set of nonorthogonal eigenfunctions (Reddy et al. 1993). Consequently, the temporal behavior of $G(t)$ substantially deviates from the temporal behavior of $g(t)$. Any conclusions drawn from λ_r can easily misrepresent the general disturbance behavior over the course of time, and the dynamics of the least stable mode are, at worst, entirely irrelevant to the temporal behavior of the linear system at finite time.

Systems governed by non-normal matrices can exhibit a large transient amplification of energy contained in the initial condition. A simple geometric example illustrates this (**Figure 2**). Assume a unit-length initial condition **f**, represented in a nonorthogonal eigenvector basis. As time progresses the eigenvector components decrease by 20% and 50%, respectively, over each time interval depicted in **Figure 2**. The vector **f** transiently increases in length and aligns itself with the least stable eigenvector direction. Only in the large-time limit will **f** decrease to zero. It is important to realize that the nonorthogonality of the eigenvector basis is a crucial component in the short-time amplification of the norm of **f**. It is equally important to acknowledge that any conclusions drawn from the decay rates along the eigenvector directions misrepresent the dynamics of the motion illustrated in **Figure 2** as they only describe the asymptotic fate of **f**, but fail to capture its transient behavior.

This simple geometric example of transient growth induced by a superposition of exponentially decaying nonorthogonal eigenvectors equally applies to the description

of disturbance behavior governed by the Navier-Stokes equations. The linearized Navier-Stokes equations for plane Poiseuille flow are non-normal; the eigenvectors form a nonorthogonal set. Following the argument above, large transient growth of energy is possible even in a parameter regime where all eigenvalues are confined to the stable half-plane, thus predicting large-time asymptotic decay.

To capture the true behavior of infinitesimal disturbances the analysis has to concentrate on the norm of the matrix exponential $G(t)$, which carries the full dynamical information without any restrictive assumptions. In the large-time limit, this analysis recovers the least stable mode; for intermediate time, however, the dynamics and spatial pattern selection may be significantly different.

Just as eigenvalues are used to quantitatively describe the asymptotic $t \to \infty$ behavior, one needs to introduce a different quantity to describe the behavior for $t = 0^+$. A simple expansion of the energy growth rate about $t = 0^+$, using the matrix exponential solution above, yields the following result (Farrell & Ioannou 1996a, Schmid & Henningson 2001, Trefethen & Embree 2005):

$$\max_{\mathbf{q}} \frac{1}{\|\mathbf{q}\|^2} \left. \frac{d\|\mathbf{q}\|^2}{dt} \right|_{t=0^+} = \max_{\mathbf{q}} \frac{1}{\|\mathbf{q}\|^2} \frac{d}{dt} \left\| \mathbf{C}(\mathbf{I} + \mathbf{A}t + \mathbf{A}^2 \frac{t}{2!} + \cdots)\mathbf{B}\mathbf{q}_0 \right\|^2 \Big|_{t=0^+} \tag{2.5a}$$

$$= \lambda_{\max}\left(\frac{1}{2}(\mathbf{Q}^H + \mathbf{Q})\right), \tag{2.5b}$$

with $\mathbf{Q} = \mathbf{CAB}$ and $\lambda_{\max}(\cdot)$ denoting the largest eigenvalue. The quantity $\lambda_{\max}(\mathbf{Q}^H + \mathbf{Q})/2$ is often referred to as the numerical abscissa (Trefethen & Embree 2005). It can alternatively be computed by determining the boundary of the numerical range of $\mathbf{Q}$ (Horn & Johnson 1991). The maximum protrusion of the numerical range into the unstable half-plane is equivalent to the numerical abscissa and thus determines the maximum energy growth at $t = 0^+$. In **Figure 3*b***[1] the boundary of the numerical range is displayed as the red line; it reaches into the unstable half-plane, and its maximum protrusion (indicated by the red dot) can be computed using Equation 2.5b.

With eigenvalues describing the asymptotic limit ($t \to \infty$) and the numerical abscissa governing the energy growth for $t = 0^+$, one may ask whether a third set in the complex plane can give information about the maximum transient energy growth. An extension of eigenvalues, known as ε-pseudospectra (Trefethen 1997), fills this role, although only in an approximate sense. The ε-pseudospectra are defined as regions in the complex plane, parameterized by ε, where the resolvent norm $\|\mathbf{C}(z\mathbf{I} - \mathbf{A})^{-1}\mathbf{B}\|$ is larger than $1/\varepsilon$. An alternative definition states that ε-pseudoeigenvalues are exact eigenvalues of the operator $\mathbf{A}+\mathbf{E}$, where $\mathbf{E}$ is a random perturbation of norm ε. The usual spectrum is recovered as ε tends to zero (Trefethen 1997, Trefethen & Embree 2005).

[1]Rather than considering the eigenvalues $\{\lambda\}$ of $\mathbf{A}$, it is customary in hydrodynamic stability theory to visualize the complex frequencies $\{\omega\}$ stemming from an assumed temporal behavior of the form $\sim \exp(-i\omega t)$. This convention yields asymptotically unstable modes when at least one complex frequency ω lies in the upper half-plane ($\omega_i > 0$), which is equivalent to finding at least one eigenvalue of $\mathbf{A}$ in the right half-plane ($\lambda_r > 0$). To avoid confusion, the unstable domain is shaded gray when spectra are displayed.

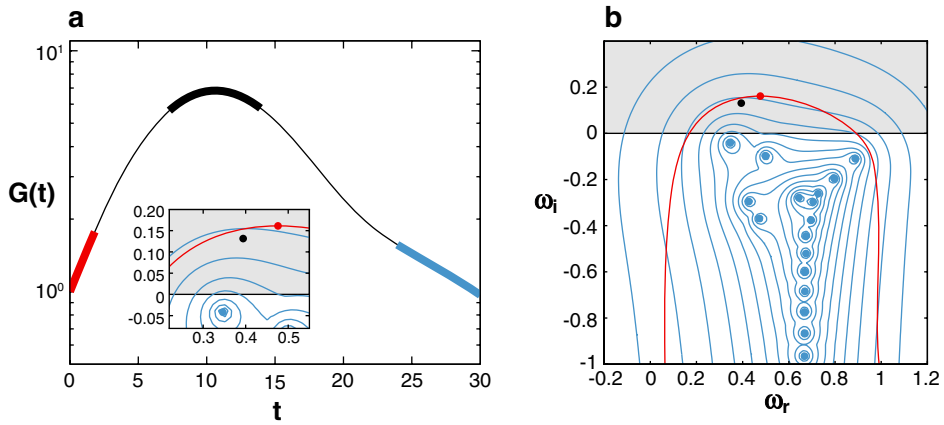

Figure 3

Transient growth of perturbation energy for two-dimensional plane Poiseuille flow at $Re = 1000$ and $\alpha = 1$. (*a*) Energy growth vs time. (*b*) Contour plot (*blue lines*) of the resolvent norm. The contour levels are $10^{0.25}, 10^{0.5}, \ldots, 10^{4}$. The eigenvalues ω (*blue dots*) predict asymptotic decay as all of them are confined to the stable half-plane. The red line denotes the boundary of the numerical range. The red dot represents the numerical abscissa, i.e., the point of maximum protrusion of the numerical range into the unstable half-plane. The black dot indicates the location in the complex plane that results in the Kreiss constant (see text); this location provides a lower bound for the maximally achievable energy amplification over time. The inset in (*a*) together with the colored lines illustrates the significance of the various spectral variables during various stages of the temporal evolution of the energy growth.

Figure 3*b* shows the three sets—spectrum, ε-pseudospectrum, numerical range—for two-dimensional plane Poiseuille flow. The boundary of the numerical range is indicated in red; the ε-pseudospectrum is visualized by contours of the resolvent norm for various values of ε; the eigenvalues are displayed as blue symbols. Various conclusions can be drawn from this figure: All eigenvalues are confined to the stable half-plane, thus predicting asymptotic decay according to the least stable eigenvalue. The numerical range protrudes into the unstable half-plane, which indicates that energy growth can be expected for small times. Finally, a lower bound for the maximum attainable transient growth in time can be deduced by measuring the amount by which the resolvent contours extend into the unstable half-plane. For example, if for some z with $\mathrm{Re}(z) = 0.1$ the resolvent norm $\|\mathbf{C}(z\mathbf{I} - \mathbf{A})^{-1}\mathbf{B}\|$ is 10^2, transient energy growth of at least $(0.1 \times 10^2)^2 = 10^2$ should be expected. To be more precise (Trefethen & Embree 2005), a constant, known as the Kreiss constant $\mathcal{K}$, can be defined according to $\mathcal{K} = \sup_{\mathrm{Re}(z)>0} \mathrm{Re}(z)\|\mathbf{C}(z\mathbf{I}-\mathbf{A})^{-1}\mathbf{B}\|$, which can be used to provide a lower estimate for the maximum amplification of energy over time, i.e., $\max_{t>0} G(t) \geq \mathcal{K}^2$. The black dot in **Figure 3*b*** shows the location in the complex plane that results in the Kreiss constant $\mathcal{K}$.

Figure 3*a*, which displays the maximum energy growth $G(t)$, confirms our predictions: We observe an initial growth of energy (with a slope given by the numerical abscissa), culminating in a peak near $t = 10$ bounded from below by the square of

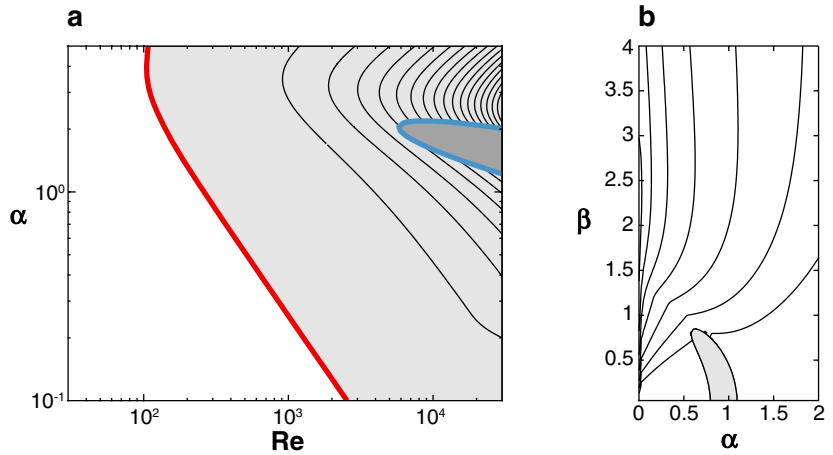

Figure 4

Parameter study of transient growth for two- and three-dimensional plane Poiseuille flow. (*a*) The neutral curve of two-dimensional plane Poiseuille flow (*blue line*) delimiting the area of asymptotic growth (*dark gray*) from the area of asymptotic decay (*light gray and white*), and the curve (*red line*) delimiting the area of transient growth, but asymptotic decay (light gray) from the area of no transient growth (*white*). The well-known critical Reynolds number $Re_{\mathrm{crit}} = 5772$ can be easily determined from the graph. In the light gray area, the contour levels of $G_{\max}$ range from 10 to 170 in steps of 10. (*b*) Maximal transient growth of energy for plane Poiseuille flow at $Re = 10000$ as a function of the streamwise (α) and spanwise (β) wave number. The largest transient growth occurs for perturbations with no streamwise dependence ($\alpha = 0$). The gray area in the $\alpha - \beta$-plane indicates parameter combinations for which asymptotic exponential growth is found. The contour levels are 250, 500, 1000, 2000, . . . , 16000.

the Kreiss constant $\mathcal{K}$, which is ultimately followed by exponential decay given by the least stable eigenvalue.

Varying the governing parameters, in particular the streamwise wave number α and the Reynolds number Re, and evaluating the maximum transient growth $\max_{t>0} G(t)$ produces **Figure 4*a***. Not only do we reproduce the familiar neutral curve (blue line), delineating parameter combinations for which an eigenvalue crosses into the unstable half-plane, we also observe a second (red) line separating parameter combinations for which the numerical range crosses into the unstable half-plane. The smallest Reynolds number for which an unstable eigenvalue is encountered is the well-known critical Reynolds number $Re_{crit} = 5772$; the largest Reynolds number below which the initial perturbation energy for two-dimensional disturbances decays monotonically is given by $Re_{ener} = 89$. The latter Reynolds number has traditionally been determined using energy stability theory (Joseph 1976). For Reynolds numbers that fall between Re_{ener} and Re_{crit}, significant transient growth (eventually followed by asymptotic decay) prevails (Reddy et al. 1993).

Note that, for normal systems, the numerical range and the spectrum cross into the unstable half-plane at the same Reynolds number. Thus, the two critical Reynolds

numbers coincide, i.e., $Re_{crit} = Re_{ener}$. This is, for example, the case for Rayleigh-Bénard convection. Although not a necessary feature, the wide gap between Re_{crit} and Re_{ener} is characteristic of many non-normal fluid systems (Schmid & Henningson 2001, Trefethen & Embree 2005).

For three-dimensional perturbations, traditional stability theory (Drazin & Reid 1981) states that for each unstable three-dimensional perturbation a spanwise independent unstable perturbation can be found at a lower Reynolds number. This statement, known as Squire's theorem, has generally led to an over-emphasis on two-dimensional studies. Evaluating the potential for transient energy growth reveals a different picture. Even though perturbations without a spanwise dependence exhibit the largest exponential growth, it is the streamwise independent disturbances (which are asymptotically stable at all Reynolds numbers) that best exploit the transient amplification of energy (**Figure 4*b***). The transient energy growth can reach many orders of magnitude—certainly significant enough to dominate the selection of coherent flow structures (Reddy & Henningson 1993).

Given that the function $G(t)$ describes the energy amplification maximized over all possible initial conditions, it is interesting to ask which specific initial perturbation is responsible for the maximum amplification $G(T)$ at a given time T. This initial condition is easily recovered via a singular value decomposition of the matrix exponential evaluated at time $t = T$ (Trefethen & Embree 2005).

2.4. Response to External Forcing

The general solution (Equation 2.2) to the governing equation (Equation 2.1) has two components: the homogeneous solution, which incorporates the effects of initial conditions, and the particular solution, which describes the influence of external forcing. Both parts fully describe the general dynamics of perturbations. Physically, the particular solution provides a model for receptivity processes. The external forcing may represent free-stream turbulence, wall roughness, or other nonsmooth geometries, body forces, or even neglected terms, such as nonlinearities, in the governing equations (Equation 2.1). The study of particular solutions then quantifies the outside influence on disturbance growth, resonance behavior, and pattern selection. Although Equation 2.2 is valid for arbitrary temporal forcing, we only consider the special cases of time-harmonic, impulsive, and stochastic external forcing.

In the time-harmonic case, the mapping of the input forcing $\mathbf{q}_{in} = (u_{in}, v_{in}, w_{in})^T$ onto the long-term output response $\mathbf{q}_{out} = (u_{out}, v_{out}, w_{out})^T$ is given, according to the Fourier transform of Equation 2.1, by the resolvent $\mathbf{C}(i\omega\mathbf{I} - \mathbf{A})^{-1}\mathbf{B}$ with ω as the forcing frequency. Define the maximum response $R(\omega)$ as the ratio of the energy of the output response to the energy of the input forcing, optimized over all possible spatial forcing profiles (Trefethen et al. 1993):

$$R(\omega) = \max_{\mathbf{q}_{in}} \frac{\|\mathbf{q}_{out}(t)\|^2}{\|\mathbf{q}_{in}\|^2} = \max_{\mathbf{q}_{in}} \frac{\|\mathbf{C}\,(i\omega\mathbf{I} - \mathbf{A})^{-1}\,\mathbf{B}\mathbf{q}_{in}\exp(i\omega t)\|^2}{\|\mathbf{q}_{in}\|^2} \tag{2.6a}$$

$$= \|\mathbf{C}\,(i\omega\mathbf{I} - \mathbf{A})^{-1}\,\mathbf{B}\|^2. \tag{2.6b}$$

This result should be contrasted to the familiar measure of response behavior based on spectral theory: the shortest distance of the forcing frequency to the eigenvalues

of the forced system. Resonance is expected as the forcing frequency ω approaches an eigenvalue of the matrix $\mathbf{A}$. According to the eigenvalue decomposition of $\mathbf{A}$

$$R(\omega) = \|\mathbf{C}\,(i\omega\mathbf{I} - \mathbf{A})^{-1}\,\mathbf{B}\|^2 = \|\mathbf{C}\mathbf{V}\underbrace{(i\omega\mathbf{I} - \Lambda)^{-1}}_{\substack{\text{spectral}\\ \text{analysis}}}\mathbf{V}^{-1}\mathbf{B}\|^2. \tag{2.7}$$

As in the case of the matrix exponential norm (Equation 2.4), the simplified spectral analysis ignores all information contained in the eigenvector structure $\mathbf{V}$. It gives a criterion for a large response based on eigenvalues only. For normal matrix operators $\mathbf{A}$ this is appropriate; for nonnormal matrices, however, large resonant behavior to external excitation can be observed even though the forcing frequency is nowhere near an eigenvalue of $\mathbf{A}$. This phenomenon is referred to as pseudoresonance (Trefethen et al. 1993). The specific spatial shape of the forcing $\mathbf{q}_{in}$ can be recovered via a singular value decomposition (Schmid & Henningson 2001).

2.5. Componentwise Transfer Function

The resolvent introduced above is closely related to the concept of a transfer function. Transfer functions are commonly used in control theory (Skogestad & Postlethwaite 1996) to describe the relation between inputs and outputs of a linear time-invariant (LTI) system, and the zeros and poles of transfer functions determine the long-time dynamic behavior of linear systems. The resolvent above is now recast in terms of the transfer function to further probe the response of infinitesimal disturbances to external harmonic excitation (Jovanović & Bamieh 2005). According to Equation 2.1, the transfer function is given by

$$\mathcal{H}(\alpha, \beta, \omega) = \mathbf{C}\,(i\omega\mathbf{I} - \mathbf{A})^{-1}\,\mathbf{B} \qquad \text{so that} \qquad \mathbf{q}_{out} = \mathcal{H}(\alpha, \beta, \omega)\,\mathbf{q}_{in}. \tag{2.8}$$

The decision of what measure to use to quantify the transfer function is important. In this case, we are interested in the worst-case amplification of deterministic inputs. For this reason, $\mathcal{H}$ is maximized over all temporal frequencies ω and all wall-normal shapes. The latter is accomplished by taking the norm. We thus define

$$\|\mathcal{H}\|_\infty(\alpha, \beta) = \max_{-\infty<\omega<\infty} \sigma_{\max}(\mathcal{H}), \tag{2.9}$$

where $\sigma_{\max}(\cdot)$ denotes the largest singular value. The above measure is referred to as the H_∞-norm (Zhou et al. 1996), indicated by the $_\infty$ subscript. As previously seen, the worst possible shape of the external forcing $\mathbf{q}_{in}$ at the worst frequency may be recovered by performing a singular value decomposition.

The H_∞-norm of the transfer function contains a great deal of information and allows a detailed analysis of the response to external influences. In particular, a componentwise analysis (Jovanović & Bamieh 2005), which restricts the input and output variables to predetermined components of the state vector, gives significantly more insight into the underlying mechanisms of the observed disturbance dynamics. For example, to probe the influence of perturbations in the wall-normal velocity on streamwise disturbances, the operators $\mathbf{B}$ and $\mathbf{C}$ in Equation 2.8 need to be modified

according to

$$\mathbf{B}_v = \begin{pmatrix} 0 & \mathbf{M}^{-1}k^2 & 0 \\ 0 & 0 & 0 \end{pmatrix}, \qquad \mathbf{C}_u = \begin{pmatrix} \frac{i\alpha}{k^2}\mathbf{D} & -\frac{i\beta}{k^2} \\ 0 & 0 \\ 0 & 0 \end{pmatrix}. \tag{2.10}$$

The $\mathcal{H}_{v\to u}$ component of the transfer function, $\mathbf{C}_u(i\omega\mathbf{I}-\mathbf{A})^{-1}\mathbf{B}_v$, can then be computed with this choice of operators. According to the magnitude of the nine components of the transfer function, important information about specific velocity components, as well as evidence for the dominance of particular flow structures, can be gained (Jovanović & Bamieh 2005). **Figure 5** displays the H_∞-norm of the nine components of the transfer function as a function of the streamwise and spanwise wave number. A logarithmic scaling and the same color map has been used for all subplots to allow a quantitative comparison. In addition, the largest response within each subplot is indicated by a black dot.

Among the nine possible combinations, the largest response by far is observed in the streamwise velocity component when forced by either the normal or spanwise component. The maximum amplification of external excitations in these components is exhibited in streamwise independent flow structures. These structures are commonly referred to as streaks. From this information, one can identify a viable and efficient mechanism that transforms low-amplitude streamwise vortices (v-w-input) into large-energy streaks (u-output) and favors the emergence of coherent flow patterns elongated in the streamwise direction (Reddy & Henningson 1993). Any other mechanism, such as the one based on oblique waves (dominant for spanwise velocities forced by spanwise perturbations, $\mathcal{H}_{w\to w}$) or the one involving a Tollmien-Schlichting wave (dominant for normal velocities forced by streamwise perturbations, $\mathcal{H}_{u\to v}$), shows maximum amplification factors at least an order of magnitude smaller. Thus, it is not normally observed, unless specific constraints are enforced in numerical simulations or physical experiments.

The dominance of streamwise elongated structures, emerging via a transient mechanism from streamwise vorticity, stands in stark contrast to classical results from modal stability analysis, which predicts the prevalence of Tollmien-Schlichting waves. Experimental observations (e.g., Alfredsson & Matsubara 2000), as well as direct numerical simulations (e.g., Berlin & Henningson 1999, Jacobs & Durbin 2001), of many wall-bounded shear flows, however, provide abundant evidence for the streamwise-vortices-streaks scenario under natural conditions.

2.6. Impulse Response

The H_∞-norm of the transfer function, split in its various components, furnishes a rich and interesting picture of energy amplifications caused by external disturbances. This information is displayed after a Fourier transform in space (wave vector) and time (frequency). An alternative, and equivalent, representation of the same information in physical space and time is given by the impulse response of the system described in Equation 2.1 (Jovanović & Bamieh 2001). Mathematically, this impulse response is

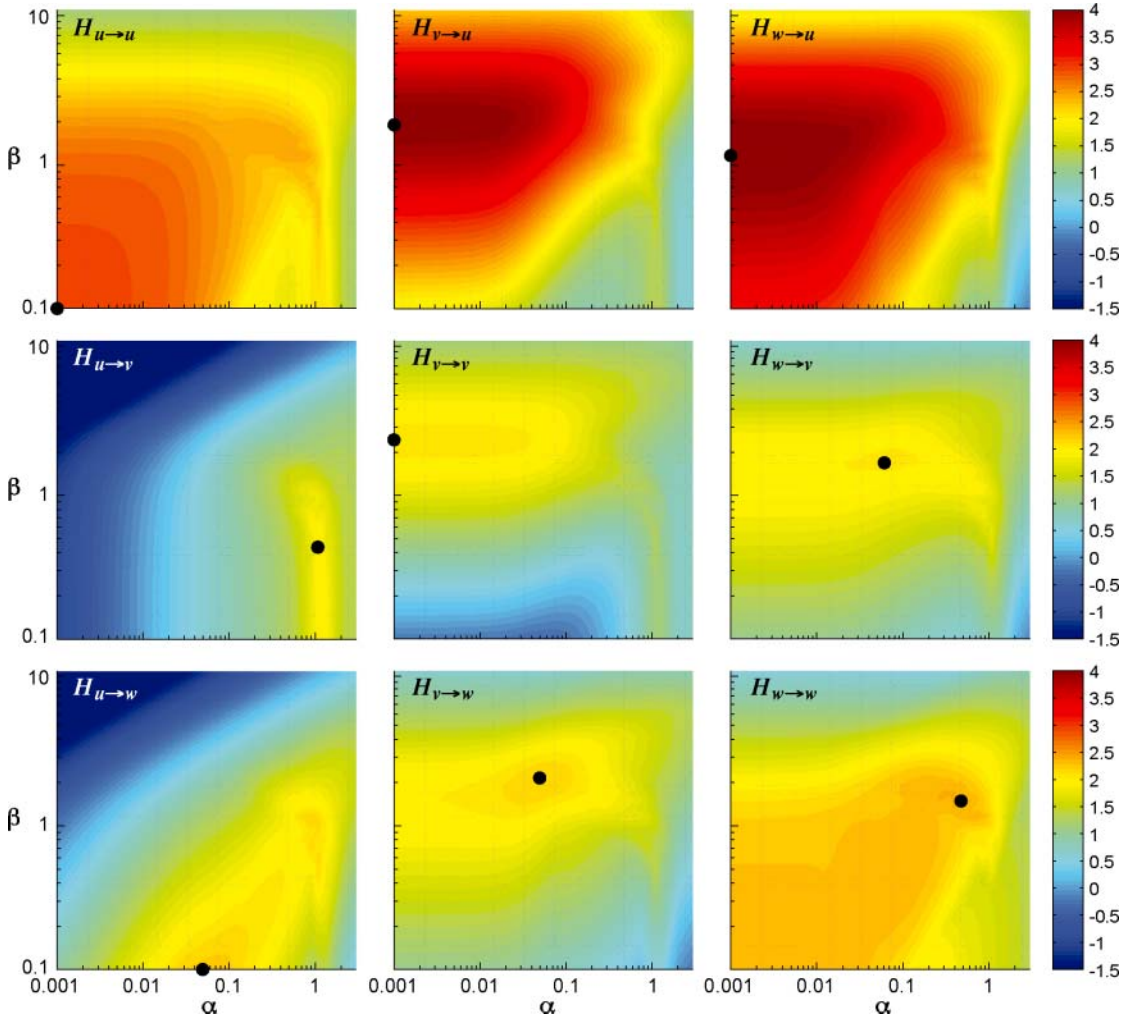

Figure 5

Componentwise H_∞-norm of the transfer function (logarithmic scaling) as a function of the streamwise (α) and spanwise (β) wave number for plane Poiseuille flow at $Re = 2000$. In each of the nine plots the black dot indicates the largest H_∞-response to harmonic external forcing. The largest response is observed in a forcing scenario that converts perturbations in the v- and w-components into perturbations in the streamwise u-component. Other combinations show markedly lower response amplitudes.

the Green's function of the linear system. By choosing $\mathbf{q}_{in} = (\delta(x), \delta(y-y_0), \delta(z))^T \delta(t)$ and applying an inverse Fourier transform back to physical space, we obtain

$$\begin{pmatrix} u_{out} \\ v_{out} \\ w_{out} \end{pmatrix} = \frac{1}{4\pi^2} \iint \mathbf{C} \exp\left[i\left(\alpha \frac{x}{t} + \beta \frac{z}{t} - i\mathbf{A} \right) t \right] \mathbf{B} \delta(y - y_0)\, d\alpha\, d\beta. \qquad (2.11)$$

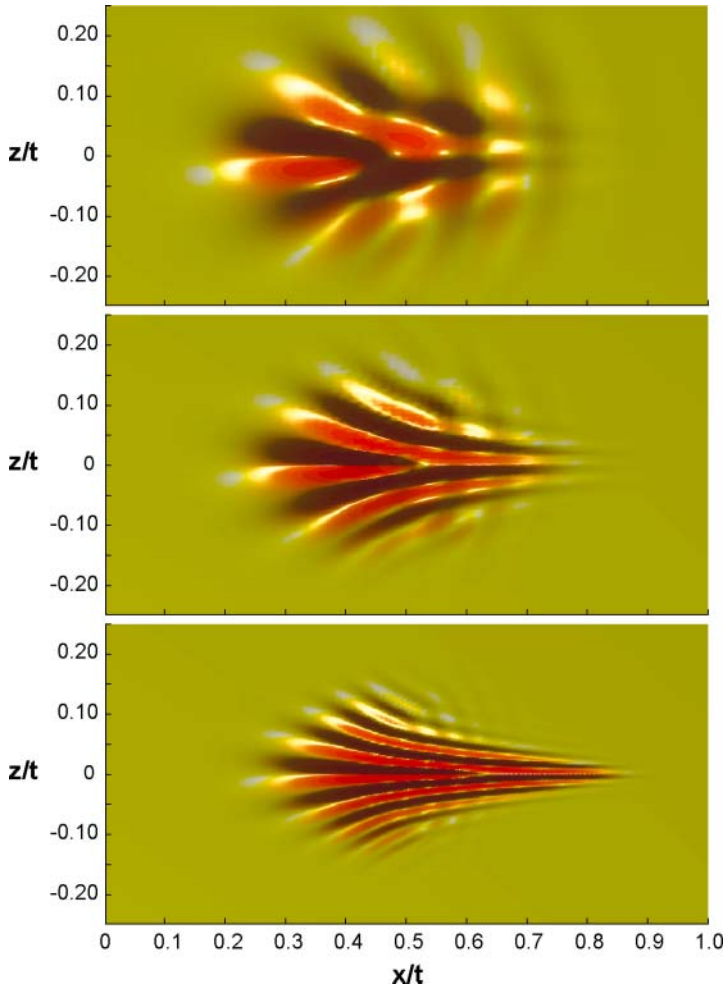

Figure 6

Impulse response (visualized using the streamwise velocity component) for plane Poiseuille flow at $Re = 1000$ at time $t = 30$ (top), $t = 60$ (middle), and $t = 120$ (bottom). The predominance of streamwise elongated structures inside the wave packet is demonstrated.

A numerical evaluation of the impulse response for plane channel flow is depicted at three representative times in **Figure 6**. The evolution of a localized wave packet displays an interior structure that is clearly dominated by streamwise elongated structures. These features are the most amplified, according to the frequency response (**Figure 5**). As time progresses, streaky structures eventually decay; in the short term, however, they govern the disturbance dynamics within the regime of validity of linear theory.

Only in the limit $t \to \infty$ can the operator **A** be replaced by its largest eigenvalue. The argument of the matrix exponential then reduces to $i\Psi t$ with $\Psi = \alpha x/t + \beta z/t - \omega_{\max}(\alpha, \beta)$, and the resulting integral can be evaluated asymptotically by the method of steepest descent (Bender & Orszag 1978). This evaluation requires the deformation of the integration path through a saddle point or, more precisely, a pinch

point (Briggs 1964, Chomaz 2005, Huerre & Monkewitz 1990), the position of which in the complex ω-plane determines the convective or absolute instability character of the underlying flow. Absolutely unstable flows typically display upstream propagating disturbances emanating from an impulsive point source. For plane Poiseuille flow, the wave packet propagates downstream, thus indicating a convective stability behavior.

The analysis of absolutely or convectively unstable flow behavior has traditionally been performed semianalytically, based on the numerical computation of the dispersion relation of the underlying flow. The numerical evaluation of the impulse response, i.e., the Green's function, of the flow and its subsequent analysis regarding propagation direction was introduced by Delbende et al. (1998) and has since been applied to a variety of open flows (see Brandt et al. 2003, Gallaire et al. 2006, Le Gal & Croquette 2000, Ravier et al. 2006).

It is worth pointing out that the internal structure of the wave packet is reminiscent of the structures observed in turbulent spots (Riley & Gad-el Hak 1985). Although the scales deviate quantitatively from experiments and numerical simulations of spots, the emergence of streaky structures may be attributed to a strong underlying linear mechanism that is radically different from the classical Tollmien-Schlichting wave framework (Gaster & Grant 1975).

2.7. Summary of Nonmodal Stability Tools

In summary, the nonmodal stability analysis based on the matrix exponential, the resolvent (or ε-pseudospectra), the numerical abscissa, the transfer function norm in component form, and the impulse response, provides a consistent and relevant description of general disturbance behavior for a large variety of fluid flows. It equally brings out the rich behavior of the dynamics governed by nonnormal linear operators and the shortcomings of trying to describe this same behavior through conventional eigenvalue analysis only. As such, these tools, although computationally more involved, represent a valuable compendium of techniques to conduct hydrodynamic stability calculations.

3. TIME-DEPENDENT FLOWS: ADJOINT FIELDS AND FUNDAMENTAL SOLUTION OPERATORS

Traditional stability analysis relies on the existence of a steady base flow solution about which perturbations are superimposed. In many realistic situations, this assumption is violated, but the characteristics of infinitesimal disturbances superimposed on a time-varying flow may still be of great importance and interest. Because we do not rely on a modal approach, the concepts introduced in the previous section may readily be generalized if a few modifications are made. In this section, we focus on a general framework for describing disturbance growth in time-varying base flows.

3.1. Variational Formulation and Adjoint Fields

One of the more common techniques to treat the stability of unsteady flows has been based on a reformulation of the optimal energy growth condition in terms

of a variational principle. Standard optimization techniques (for example, conjugate gradient algorithms) can then be employed to arrive at an optimal condition in an iterative manner. The optimization process should respect the constraints given by the governing equations; in other words, the admissible flow fields have to satisfy the linearized Navier-Stokes equations and the specified boundary and initial conditions. These constraints are enforced via Lagrange multipliers. Because the constraints have to be enforced locally, rather than globally, the Lagrange multipliers are time- and space-dependent fields governed by a complementary set of differential equations, known as the adjoint equations (Hill 1995).

For stability problems, we are interested in the maximum amplification of energy over a given time span $0 \leq t \leq T$. The ratio of disturbance energy at time T to the initial energy then serves as a cost functional that needs to be maximized by adjusting the spatial shape of the initial condition. An augmented Lagrangian, consisting of this cost functional as well as the constraints, is then defined in the form

$$\mathcal{L}(\mathbf{q}, \tilde{\mathbf{q}}, \mathbf{q}_0, \tilde{\mathbf{q}}_0) = \frac{\|\mathbf{q}(T)\|^2}{\|\mathbf{q}_0\|^2} - \int_0^T \tilde{\mathbf{q}}^H \mathbf{C}\left(\frac{d}{dt} - \mathbf{A}\right)\mathbf{B}\mathbf{q}\, dt - \tilde{\mathbf{q}}_0^H(\mathbf{q}(0) - \mathbf{q}_0). \tag{3.1}$$

The first term represents the cost functional to be maximized, i.e., the ratio of disturbance energy after T time units and the initial energy. The second and third terms are introduced to enforce the governing equations and initial conditions, respectively. These latter terms are premultiplied by two variables, $\tilde{\mathbf{q}}$ and $\tilde{\mathbf{q}}_0$, which add a penalty to the Lagrangian $\mathcal{L}$ if $\mathbf{q}$ does not satisfy Equation 2.1 or $\mathbf{q}(0)$ does not conform to the initial conditions $\mathbf{q}_0$. The two adjoint variables therefore act as sensitivities measuring, in the case of $\tilde{\mathbf{q}}$, the influence of momentum sources in the governing equations and, in the case of $\tilde{\mathbf{q}}_0$, the expected change in $\mathcal{L}$ due to variations in the initial conditions (Hill 1995).

Setting to zero the first variations of $\mathcal{L}$ with respect to its independent variables $\mathbf{q}, \tilde{\mathbf{q}}, \mathbf{q}_0, \tilde{\mathbf{q}}_0$ yields the following set of equations:

$$\frac{\delta\mathcal{L}}{\delta\tilde{\mathbf{q}}} = 0 \rightarrow \mathbf{C}\left(\frac{d}{dt} - \mathbf{A}\right)\mathbf{B}\mathbf{q} = 0, \tag{3.2a}$$

$$\frac{\delta\mathcal{L}}{\delta\mathbf{q}} = 0 \rightarrow \mathbf{B}^H\left(\frac{d}{dt} + \mathbf{A}^H\right)\mathbf{C}^H\tilde{\mathbf{q}} = 0, \tag{3.2b}$$

$$\left.\begin{aligned}\frac{\delta\mathcal{L}}{\delta\tilde{\mathbf{q}}_0} &= 0\\ \frac{\delta\mathcal{L}}{\delta\mathbf{q}_0} &= 0\end{aligned}\right\} \rightarrow \begin{cases}\mathbf{q}(0) = \dfrac{\|\mathbf{q}_0\|^4}{2\|\mathbf{q}(T)\|^2}\tilde{\mathbf{q}}(0),\\ \tilde{\mathbf{q}}(T) = \dfrac{2}{\|\mathbf{q}_0\|^2}\mathbf{q}(T),\end{cases} \tag{3.2c}$$

which is amenable to an iterative solution procedure. During one cycle of this process, the governing equations are integrated forward in time using a given initial condition. At time $t = T$, the output of this integration $\mathbf{q}(T)$ is converted into a terminal condition $\tilde{\mathbf{q}}(T)$ for the adjoint equations which are subsequently solved backward in

time to produce $\tilde{\mathbf{q}}(0)$, from which a new initial condition $\mathbf{q}(0)$ for the direct problem is determined. This process continues until convergence is reached.

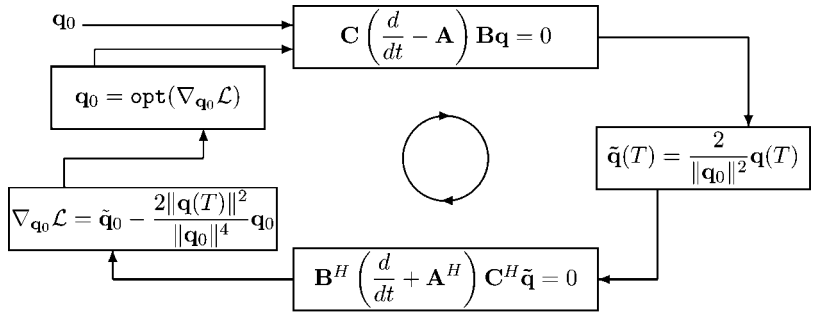

SKETCH OF ITERATIVE SCHEME

The final result is the initial condition that maximizes the amplification of energy over a time interval $0 \le t \le T$, from which the maximum transient energy growth is readily determined. To avoid numerical difficulties and to ensure proper convergence for a wide range of parameters, robust optimization techniques (such as conjugate gradient methods) have to be used (Nocedal & Wright 2000). In this case, the gradient of the Lagrangian with respect to the initial condition, $\nabla_{\mathbf{q}_0}\mathcal{L}$, is computed and used as input to a standard optimization routine (abbreviated as `opt( )` in the sketch above).

It is important to realize that by varying the time T over which the optimization is performed, the above procedure yields the maximum growth curve $G(t)$; however, no steady base flow has to be assumed because the forward (and backward) integration of the governing (and adjoint) equations easily accommodates a time-varying velocity profile.

The above technique has been successfully implemented in various complex flows, such as, e.g., in Corbett & Bottaro (2001), Guégan et al. (2006), Luchini & Bottaro (2001), Pralits et al. (2000).

3.2. The Fundamental Solution Operator

As an alternative to the adjoint formulation outlined in the previous section, the fundamental solution operator may be efficiently used to characterize perturbation growth superimposed on an unsteady base flow. For steady operators $\mathbf{A}$ the fundamental solution operator is the familiar matrix exponential; for nonautonomous systems, however, this operator has to be determined—or approximated—numerically. Various methods, e.g., based on the Magnus method, are available (Iserles et al. 1999). Once the fundamental solution operator $\mathbf{X}(t)$ is known, the tools of nonmodal stability analysis can easily be adapted to address the disturbance behavior for time-varying flows. It simply suffices to replace the matrix exponential $\exp(t\mathbf{A})$ by the operator $\mathbf{X}(t)$ (Farrell & Ioannou 1996b, Schmid & Kytömaa 1994). The general solution of

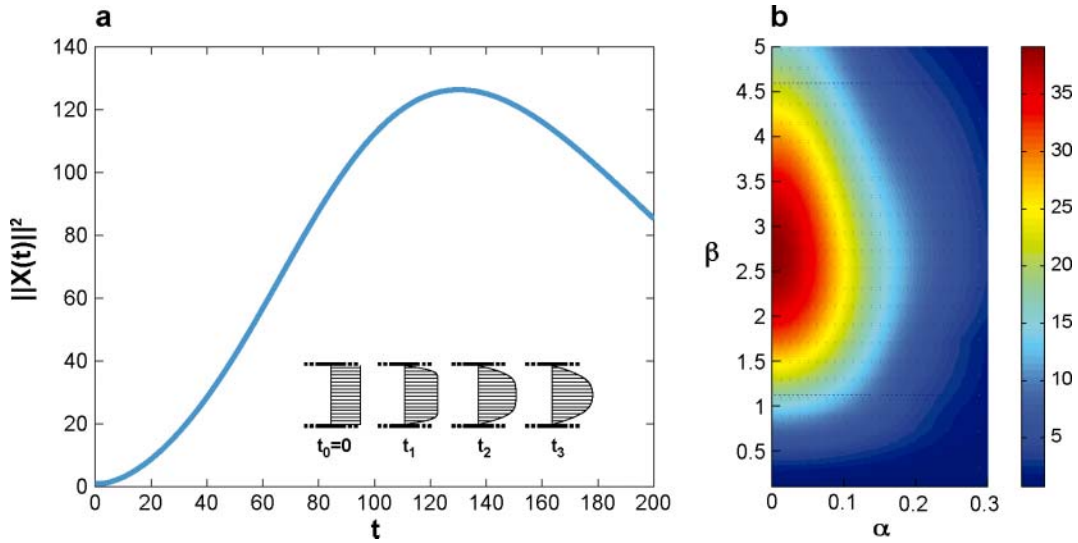

Figure 7

(*a*) Transient perturbation energy amplification for three-dimensional inlet channel flow at $Re = 1000$ with streamwise wave number $\alpha = 0$ and spanwise wave number $\beta = 2$. Constant mass flux has been enforced. The inset presents a sketch of the base flow at four distinct time instances. (*b*) Optimal energy growth over a time interval $T = 45$ as a function of the streamwise (α) and spanwise (β) wave number. The predominance of streamwise independent structures is observed.

Equation 2.1 for time-varying $\mathbf{A}(t)$ then reads

$$\begin{pmatrix} u_{out} \\ v_{out} \\ w_{out} \end{pmatrix} = \mathbf{CX}(t)\mathbf{B} \begin{pmatrix} u_0 \\ v_0 \\ w_0 \end{pmatrix} + \mathbf{CX}(t) \int_0^t \mathbf{X}^{-1}(\tau)\mathbf{B} \begin{pmatrix} u_{in}(\tau) \\ v_{in}(\tau) \\ w_{in}(\tau) \end{pmatrix} d\tau. \qquad (3.3)$$

The use of this solution is demonstrated by considering the inlet flow, which develops as uniform flow enters a parallel channel. The base flow is modeled as a time-dependent velocity profile (see inset in **Figure 7*a***) in an infinite channel. The initial stage of the base flow development is characterized by a sharp shear layer near the wall and a rather uniform flow profile in the center of the channel, which over time relaxes into a parabolic velocity profile. The mass flux across the channel is enforced to be constant. The growth of energy, maximized over all initial conditions, and given by $G(t) = \|\mathbf{CX}(t)\mathbf{B}\|^2$, is displayed in **Figure 7*a***. A significant amount of amplification is observed during the evolution of the base velocity profile from plug flow to an ultimately parabolic shape. The maximum amplification $\|\mathbf{CX}(T)\mathbf{B}\|^2$ as a function of the streamwise and spanwise wave numbers is plotted in **Figure 7*b*** at a specific time. It again demonstrates the significantly larger amplification of streamwise independent perturbations; structures elongated in the streamwise direction experience an energy amplification that is about one order of magnitude larger than the amplification of purely streamwise traveling waves over the specified time interval.

Other time-dependent configurations, such as start-up flows or relaxation flows, may be treated in a similar manner. The stability analysis of time-dependent flows requires only a modestly larger effort directed toward the computation of the fundamental solution operator $\mathbf{X}(t)$; the insight gained from the stability analysis, however, more than justifies this effort.

3.3. Floquet Theory: A Special Case

Systems characterized by a periodic time dependence, i.e., $\mathbf{A}(t+T) = \mathbf{A}(t)$, where T denotes the period, constitute a special case of time-varying flows that has attracted considerable attention. Flows of this type are ubiquitous in industrial applications, where oscillatory pressure gradients imposed by pumps or other rotating turbomachinery are nonnegligible, in coastal engineering problems concerned with sediment transport and erosion of beaches due to waves, or in biomedical applications dealing with pulmonary or circulatory flow. The substantial body of literature for time-periodic problems stems not only from the prominence of such flows in applications, but also from their mathematical tractability.

Floquet theory is the tool of choice for analyzing linear systems that involve time-periodic coefficients. According to the Floquet theorem (see Liu 2003, Verhulst 2006), the fundamental solution operator $\mathbf{X}(t)$ can be decomposed into the product of a T-periodic part $\mathbf{P}$ with $\mathbf{P}(t+T) = \mathbf{P}(t)$ and a remainder part that can be described in matrix exponential form $\exp(t\mathbf{F})$. Attention is usually focused on the amplification of disturbances over a single period. If the energy of the disturbance at the end of one period is larger than the energy at the outset, one concludes that the system is unstable. If the energy decays over one period, the system is deemed stable. Thus, common practice concentrates on the eigenvalues of $\exp(T\mathbf{F})$, referred to as the monodromy matrix. The eigenvalues $\{\mu\}$ of the monodromy matrix are known as Floquet multipliers. If at least one Floquet multiplier lies outside the unit disk, instability arises. At parameter values for which all Floquet multipliers are inside the unit disk, stability is expected. Just as eigenvalues for non-normal autonomous problems only describe the asymptotic limit of large times, the Floquet multipliers of a nonnormal monodromy matrix only predict the behavior of periodic systems in the limit of an infinite number of periods. In the same spirit as in previous sections, the full evolution operator reads

$$G(T) = \|\mathbf{C}\mathbf{P}(T)\exp(T\mathbf{F})\mathbf{B}\|^2 = \|\mathbf{C}\mathbf{P}(T)\mathbf{V}\underbrace{\exp(T\Lambda)}_{\substack{\text{spectral}\\ \text{Floquet}\\ \text{analysis}}}\mathbf{V}^{-1}\mathbf{B}\|^2. \tag{3.4}$$

Within the framework of nonmodal stability theory, a more general approach needs to be taken that does not rely exclusively on eigenvalues (or Floquet multipliers). We proceed by applying the fundamental solution operator $\mathbf{X}(t) = \mathbf{P}(t)\exp(t\mathbf{F})$ over one period and probe the maximum energy amplification $\|\mathbf{C}\mathbf{X}(t)\mathbf{B}\|^2$ over this interval. Pulsatile channel flow is chosen as a base flow. A sketch of the base profile is included as an inset in **Figure 8*a***. The maximum energy amplification shows a significant peak within one period, even though at the end of the period a more modest amplification has been accomplished. It is interesting to note that the largest rise in

energy amplification coincides with the backstroke where reverse flow is dominant. This phenomenon is in agreement with experimental (Obremski & Fejer 1967) and computational (Juarez & Ramos 2003) results, although precise quantitative studies need to be performed. Over more than one period, increasingly larger amplitudes are observed, as shown in the polar plot of **Figure 8*b*** displaying $G(t)$ over three and a quarter periods.

For the chosen parameters, all Floquet multipliers are confined to the unit disk, therefore predicting that perturbations will eventually decay to zero. The Floquet multipliers are displayed in **Figure 8*c*** together with contours of the resolvent norm $\|(z\mathbf{I} - \mathbf{CX}(T)\mathbf{B})^{-1}\|$, a representation of ε-pseudo-Floquet multipliers. Although the Floquet multipliers lie within the unit disk—thereby describing an asymptotically contracting operator $\mathbf{CX}(T)\mathbf{B}$—the resolvent contours reach the region outside the unit disk. Consequently, we conclude that short-time behavior may significantly deviate from the asymptotic fate of disturbances. This conclusion can be made more precise (Trefethen & Embree 2005) by computing the Kreiss constant $\mathcal{K}$, this time for powers of matrices. Transient energy amplification over many periods is confirmed in **Figure 8*d***; although asymptotically we observe a decay rate predicted by the least stable Floquet multiplier, a substantial amount of energy growth prevails over many periods.

In summary, two sources of nonmodal energy growth have been identified that are not captured by traditional Floquet theory: a strong amplification of energy within one fundamental period T, and a transient growth of energy from period to period that is due to the nonnormal nature of the monodromy matrix. Estimates of the latter can be derived from the ε-pseudo-Floquet multipliers.

4. ADDING UNCERTAINTY: A STOCHASTIC VIEWPOINT

In the previous sections the disturbance behavior governed by a deterministic system was investigated under the influence of deterministic forcing or deterministic initial conditions. Under realistic conditions—in natural environments or even under well-controlled laboratory conditions—a certain amount of stochastic effects should be expected. In this section, we present techniques to characterize and quantify stability properties within a statistical framework. Two stochastic scenarios are considered: (*a*) the response of a deterministic system operator $\mathbf{A}$ driven by an external stochastic process $\mathbf{q}_{in}$, and (*b*) the energy amplification potential of a system operator $\mathbf{A}$ that is perturbed by a stochastic process.

Besides the intrinsic merit of this analysis, there is a second motivation for looking at hydrodynamic stability from a stochastic point of view: It will provide a measure of the robustness of results obtained from a deterministic study. Growth rates, energy amplifications, or pattern selection principles would not carry much weight if a small perturbation, caused, for example, by low levels of external turbulence, minute wall roughness, non-negligible end-wall effects, weak compressibility, or a small perturbation in the base profile—all of them neglected in a standard analysis—would show an appreciable effect on the obtained results. Only results that are robust to reasonable levels of internal or external perturbations may be expected to be observable under

natural conditions. In this sense, a stochastic analysis of hydrodynamic stability systems adds a layer of confidence to results that have been obtained in the context of highly idealized assumptions.

4.1. External Stochastic Forcing and the Lyapunov Equation

Assume that in the governing Equation 2.1 the forcing $\mathbf{q}_{in} = (u_{in}, v_{in}, w_{in})^T$ is stochastic in nature and, to signify this change, replace the variable $\mathbf{q}_{in}$ by the stochastic

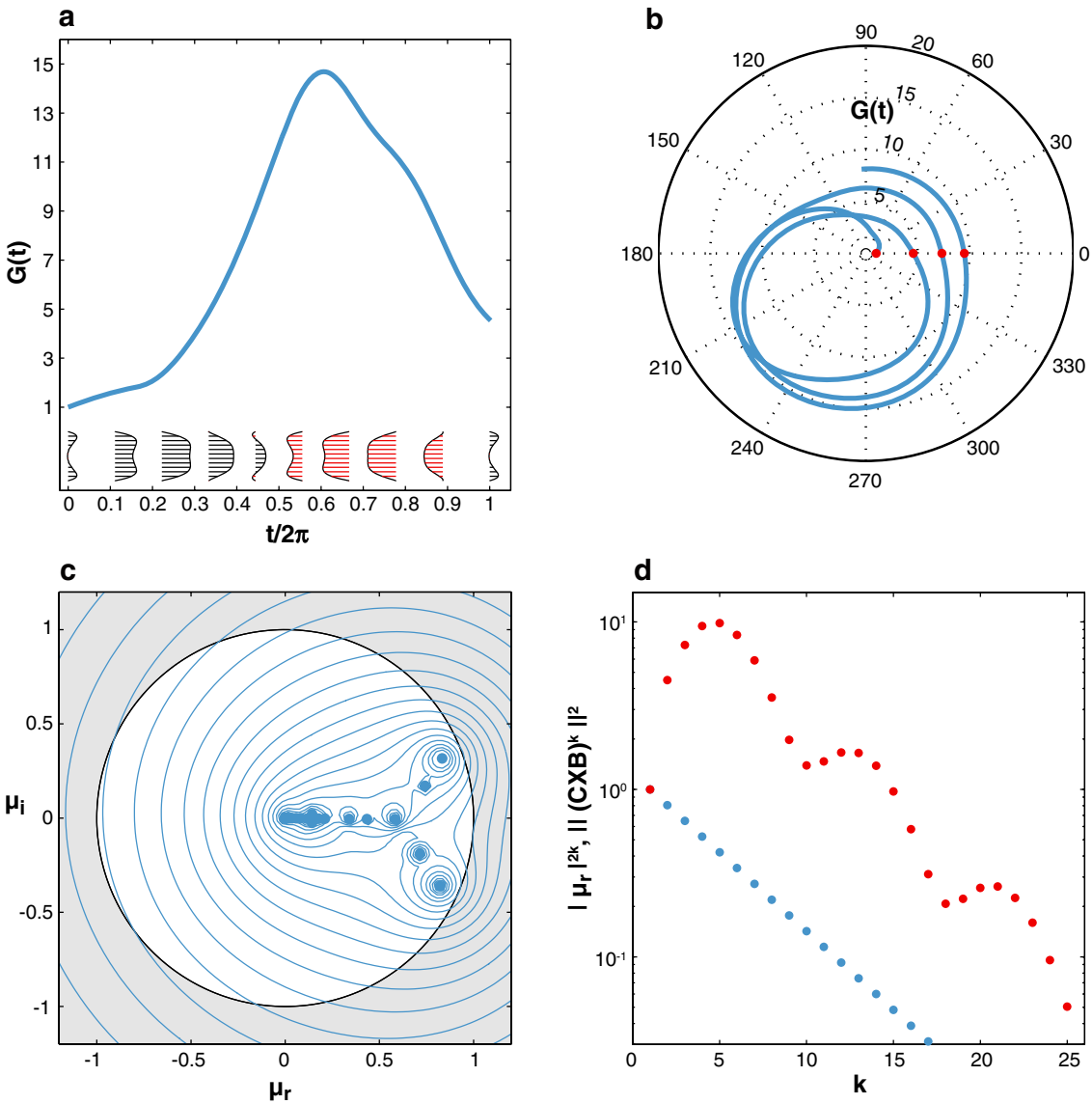

variable $\boldsymbol{\eta}(t)$ with $\langle \boldsymbol{\eta}(t_1)\boldsymbol{\eta}^H(t_2)\rangle = \mathbf{R}\delta(t_1 - t_2)$, $\langle\cdot\rangle$ denoting an ensemble average and $\mathbf{R}$ the spatial correlation matrix. With a zero initial condition, the solution of the forced problem then reads $\mathbf{q}_{out} = \mathbf{C}\int_0^t \exp((t-s)\mathbf{A})\mathbf{B}\,\eta(s)\,ds$. Due to the stochastic nature of $\mathbf{q}_{out}$, the quantitative description of the output has to involve statistical techniques. For this reason, we form the correlation matrix of the forced solution $\mathbf{q}_{out}$ to obtain (Farrell & Ioannou 1993)

$$\left\langle \mathbf{q}_{out}\,\mathbf{q}_{out}^H \right\rangle = \left\langle \mathbf{C}\int_0^t\int_0^t \exp(\mathbf{A}(t-s))\mathbf{B}\eta\,\eta^H\mathbf{B}^H\exp(\mathbf{A}^H(t-s'))\mathbf{C}^H ds'ds \right\rangle \tag{4.1a}$$

$$= \mathbf{C}\underbrace{\int_0^t \exp(\mathbf{A}(t-s))\mathbf{B}\mathbf{R}\mathbf{B}^H\exp(\mathbf{A}^H(t-s))\,ds}_{\mathbf{G}(t)}\mathbf{C}^H. \tag{4.1b}$$

The matrix $\mathbf{G}(t)$ contains the second-order statistics of the flow field. It can be computed by evaluating the integral in Expression 4.1b or, alternatively, by deriving an evolution equation for $\mathbf{G}(t)$ by differentiating Expression 4.1b with respect to time (Farrell & Ioannou 1993, Hoepffner 2006). For stable systems and in the limit of large times, the steady-state matrix $\mathbf{G}_\infty = \lim_{t\to\infty}\mathbf{G}(t)$ is governed by the algebraic Lyapunov equation

$$\mathbf{A}\mathbf{G}_\infty + \mathbf{G}_\infty\mathbf{A}^H + \mathbf{B}\mathbf{R}\mathbf{B}^H = 0 \tag{4.2}$$

from which $\mathbf{G}_\infty$ can be determined using standard numerical techniques. It is an established fact from control systems theory (Zhou et al. 1996) that the H_2-norm of the transfer function $\mathcal{H}$ defined as

$$\|\mathcal{H}\|_2^2(\alpha,\beta) = \frac{1}{2\pi}\int_{-\infty}^{\infty}\mathrm{trace}\{\mathcal{H}(\alpha,\beta,\omega)\mathcal{H}^H(\alpha,\beta,\omega)\}\,d\omega = \mathrm{trace}\{\mathbf{C}\mathbf{G}_\infty\mathbf{C}^H\} \tag{4.3}$$

bears a stochastic interpretation, as it measures the output statistics of a deterministic system to random forcing. The transfer function $\mathcal{H}(\alpha,\beta,\omega)$ has been introduced in Equation 2.8, and we observe that the choice of norm (H_∞ versus H_2) provides

Figure 8

Floquet analysis of two-dimensional pulsatile channel flow at $Re = 1200, \alpha = 1$ driven by an oscillatory pressure gradient of amplitude $P = 4$ and frequency ω. The Womersley number is $W\hat{o} = h\sqrt{\omega/\nu} = \sqrt{2}a/\delta = 5$, where δ denotes the Stokes-layer thickness and a the channel width. (*a*) Maximum transient energy amplification over one period demonstrating significant growth of disturbance energy; most of this growth is encountered during the backstroke. Base velocity profiles for selected times are given as an inset. (*b*) Maximum transient energy amplification over three and a quarter periods, displayed in polar coordinates $(r,\theta) = (G(t), 2\pi t/T)$. (*c*) Spectrum (*blue symbols*) and ε-pseudospectrum (*blue contours*) of the monodromy matrix $\mathbf{C}\mathbf{X}(T)\mathbf{B}$. The contour levels correspond to $10^{0.75}, 10^{1}, 10^{1.25}, \ldots, 10^{5}$. Even though all eigenvalues are confined to the stable domain, i.e., the unit disk, the ε-pseudospectrum protrudes into the unstable domain (*gray area*). Transient growth effects should therefore be expected in the norm of powers of the monodromy matrix. (*d*) Norm of $(\mathbf{C}\mathbf{X}(T)\mathbf{B})^k$ as a function of k confirming the transient growth of energy from period to period, before the asymptotic decay rate, predicted by the least stable Floquet multiplier, is observed. The powers of the least stable Floquet multiplier (*blue symbols*) are included for comparison. The first four red symbols in (*d*) correspond to the four red symbols in (*b*).

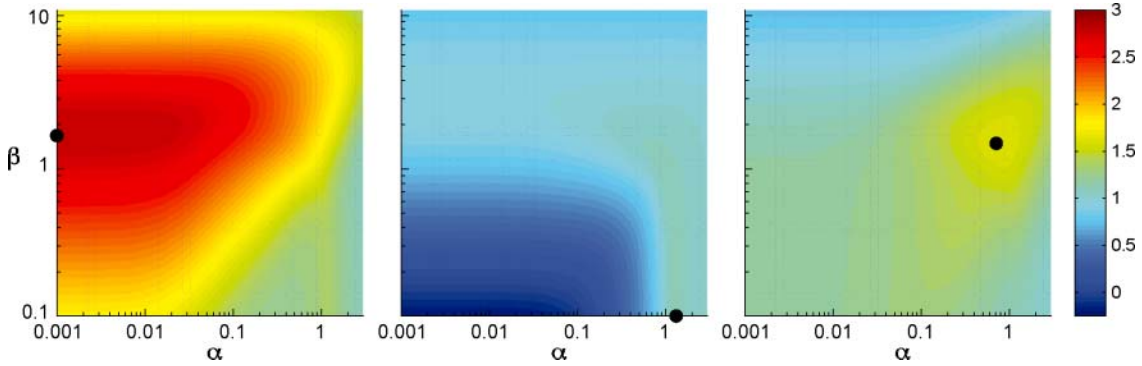

Figure 9

Componentwise H_2-norm of the transfer function (logarithmic scaling) as a function of the streamwise (α) and spanwise (β) wave number for plane Poiseuille flow at $Re = 2000$. In each of the three plots the black dot indicates the largest H_2-response to stochastic external forcing in all three momentum components. The three figures show the response to random forcing in the (*a*) streamwise, (*b*) normal, and (*c*) spanwise velocity component. The largest response is observed in the streamwise u-component. The response in the other two components is significantly lower.

a measure of either the worst-case response to harmonic forcing or the maximum variance produced by random input. The central quantity $\mathbf{G}_\infty$ needed to compute the latter is referred to as the controllability Gramian in the control literature (Skogestad & Postlethwaite 1996, Zhou et al. 1996).

The H_2-norm of the transfer function $\mathcal{H}$, computed via the Lyapunov Equation 4.2, is displayed in **Figure 9**. For stochastic perturbations in all three velocity components, the response in the streamwise, normal, and spanwise velocity is given as a function of the streamwise wave number α and the spanwise wave number β. The similarity with the deterministic case, depicted in **Figure 5**, is remarkable. The streamwise velocity component shows the largest overall response to stochastic forcing, with the peak value attained for perturbations that show a weak or vanishing streamwise dependence (Jovanović & Bamieh 2005). Other structures, and other velocity components, are much less amplified. This confirms that the conclusions drawn from an analysis of the deterministic system hold even in the presence of external stochastic excitation.

In the special case of streamwise independent perturbations, Bamieh & Dahleh (2001) exploited scaling laws and the block-triangular structure of the system matrix $\mathbf{A}$ to demonstrate that the H_2-norm of the transfer function depends cubically on the Reynolds number.

Note that the matrix $\mathbf{C}\mathbf{G}_\infty\mathbf{C}^H$ is, by construction, Hermitian. Each of its mutually orthogonal eigenvectors describes a flow pattern that contributes optimally (measured by the corresponding eigenvalue) to the variance of the statistically steady state (Farrell & Ioannou 1993, Hoepffner 2006). The eigenvalue decomposition of the matrix $\mathbf{C}\mathbf{G}_\infty\mathbf{C}^H$ is known as the Karhunen-Loève (KL), or proper orthogonal decomposition (POD), which has been applied to various turbulent flow fields (Aubry 1991, Berkooz et al. 1993, Sirovich 1987). A backward KL-decomposition can

similarly be constructed in which the forcing, rather than the output, is decomposed as to its contribution to the variance of the statistically steady state (see Farrell & Ioannou 1993).

4.2. Internal Uncertainty and Covariance Dynamics

A different kind of stochastic effect stems from uncertainties in the operator itself (Farrell & Ioannou 2002). For example, the base flow may be influenced by small fluctuations, thus compromising the assumption of a steady profile. The underlying system matrix $\mathbf{A}$ should hence be modeled as a stochastic matrix operator. For our case, we take $\mathbf{A}$ to be of the form

$$\mathbf{A}(t) = \mathbf{A}_S + \epsilon\mu(t)\mathbf{S} \tag{4.4}$$

with $\mathbf{A}_S$ denoting the statistically steady part of $\mathbf{A}$, and $\mathbf{S}$ the matrix containing the terms influenced by uncertainty. The stochastic process $\mu(t)$ is taken as $d\mu = -\nu\mu\, dt + dW$, with dW a Wiener process of zero mean and unit standard deviation. The amplitude of the stochastic perturbations is given by the parameter ϵ. The quantity ν is related to the auto-correlation time via $1/\nu$, i.e., $\langle\mu(t_1)\mu(t_2)\rangle = \exp(-\nu|t_1 - t_2|)$, and it sets the standard deviation of μ.

After some algebra (details of which are given in Farrell & Ioannou 2002), we arrive at an evolution equation for the solution

$$\frac{d}{dt}\begin{pmatrix} V \\ E \end{pmatrix} = \epsilon\mu(t)\underbrace{\exp(-\mathbf{A}_S t)\mathbf{S}\exp(\mathbf{A}_S t)}_{\mathbf{H}(t)}\begin{pmatrix} V \\ E \end{pmatrix}, \tag{4.5}$$

where V and E are defined by $\exp(\mathbf{A}_S t)(V, E)^T = (v, \eta)^T$, which, via an integrating factor, removes the solution components associated with the steady operator $\mathbf{A}_S$ and allows the concentration on uncertain effects governed by $\epsilon\mu(t)\mathbf{S}$. The fundamental solution operator $\mathbf{X}(t)$ corresponding to the time-dependent operator $\epsilon\mu(t)\,\mathbf{H}(t)$ describes the evolution of the stochastic variable $(V, E)^T$. Its mean value describes the evolution of the mean value of $(V, E)^T$ and thus $(v, \eta)^T$. It is advantageous to use a moment expansion of the solution operator $\mathbf{X}(t)$ since we can take advantage of the fact that moments beyond the quadratic one vanish for Gaussian distributions.

As discussed in the previous section, the correlation matrix $\mathbf{K}(t) = \langle\mathbf{q}\,\mathbf{q}^H\rangle$ carries second-order statistics, among them the root-mean-square values of the velocities. For uncertain systems governed by Equation 4.4, an evolution equation for the correlation matrix can be derived in the form (Farrell & Ioannou 2002)

$$\frac{d}{dt}\mathbf{K} = \Big(\mathbf{A}_S + \epsilon^2\mathbf{S}\mathbf{D}\Big)\mathbf{K} + \mathbf{K}\Big(\mathbf{A}_S^H + \epsilon^2\mathbf{D}^H\mathbf{S}^H\Big) + \epsilon^2(\mathbf{S}\mathbf{K}\mathbf{D}^H + \mathbf{D}\mathbf{K}\mathbf{S}^H) \tag{4.6}$$

with

$$\mathbf{D} = \int_0^t \exp(\mathbf{A}_S\tau)\mathbf{S}\exp(-\mathbf{A}_S\tau)\exp(-\nu\tau)\, d\tau. \tag{4.7}$$

The largest eigenvalue of $\mathbf{K}(t)$ corresponds to the largest contribution of a coherent flow structure (given by the associated eigenvector) to the variance of the uncertain system.

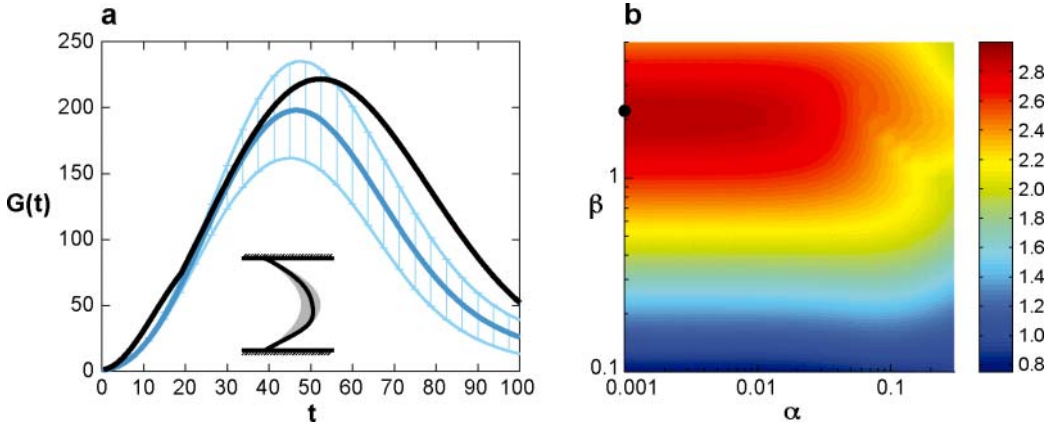

Figure 10

Energy growth of plane Poiseuille flow with a perturbed base velocity profile. The uncertainty in the base profile is given by a random superposition of four deterministic local velocity perturbations, governed by a stochastic process with $\nu = 0.2$ and $\epsilon = 0.2$ (see the inset for an instantaneous profile). The remaining parameters are $Re = 2000$, $\alpha = 0.2$, and $\beta = 2$. (*a*) The black curve shows the optimal energy growth; the blue line represents the mean of 100 Monte-Carlo simulations starting with the optimal initial condition of the unperturbed base profile at $t_{spec} = 50$. The error bars (*light blue*) indicate one standard deviation. (*b*) Maximum energy growth (using logarithmic scaling) for the above parameters as a function of streamwise and spanwise wave number, α and β, respectively. Again, a strong favoring of streamwise elongated structures ($\alpha \approx 0$) is observed, even for a stochastically perturbed base velocity profile.

To demonstrate the above, the parabolic channel flow profile is perturbed by superimposing four localized Gaussian functions multiplied by four coefficients that are governed by a temporal stochastic process $\mu(t)$ with an autocorrelation time $1/\nu = 5$ and an amplitude of $\epsilon = 0.2$. The results are shown in **Figure 10**. A significant amount of energy amplification can be observed that is confirmed by Monte-Carlo simulations starting with an optimal disturbance. A parameter study assessing the largest energy growth as a function of the streamwise and spanwise wave number shows again the dominance of streamwise elongated structures. Both statistical analyses, based on stochastic external excitation and on a stochastic perturbation of the underlying system matrix operator, have produced evidence of a remarkable robustness of a linear nonmodal mechanism that clearly favors flow patterns with a weak or vanishing streamwise dependence (**Figure 10*b***).

The same robustness cannot be claimed for the eigenvalues (spectrum) of the underlying operator. As demonstrated for many non-normal hydrodynamic stability operators, a minute perturbation added to **A** can cause the displacement of eigenvalues by orders of magnitude larger than the size of the perturbation (Reddy et al. 1993, Schmid et al. 1993, Trefethen & Embree 2005). It is important to realize that the disturbance behavior governed by the linearized Navier-Stokes equations is robust, even though its representation in terms of eigenvalues may not be.

5. FLOWS IN COMPLEX GEOMETRIES: WAVE PACKETS AND GLOBAL MODES

The assumption of a parallel base flow greatly simplifies any stability analysis, but at the same time introduces a constraint that misrepresents many realistic configurations. Even simple flows such as jets and wakes consist of a base velocity profile that varies in the normal as well as the streamwise direction. For weakly diverging flow fields, a locally parallel flow assumption within a Wentzel-Kramer-Brillouin-Jeffreys (WKBJ) framework can lead to meaningful results (Chomaz 2005). However, for highly nonparallel flows or flows in complex geometries, an alterative method of stability analysis has to be employed.

5.1. Arbitrary Spatial Dependence, Global Modes, and Their Superposition

The examples given in this review have mostly considered plane Poiseuille flow where two homogeneous coordinate directions resulted via a Fourier transform in a streamwise and spanwise wave number parameterizing the problem. For flows with multiple inhomogeneous directions, say x and y, eigenfields $\Phi(x, y)$ have to be determined together with the corresponding eigenvalues (Theofilis 2003). Even though the linear stability problem can be formulated for complex flow configurations, the size of the resulting discretized system in general becomes prohibitively large to allow for a direct calculation of the spectrum or nonmodal stability measures. At the same time, flows in complex geometries show intricate disturbance dynamics that could benefit (even more so than in simple geometries) from a systematic decomposition of the flow field and a breakdown into dynamically relevant flow structures.

Iterative techniques, borrowed from computational linear algebra, are becoming better suited to extract information from highly complex and/or three-dimensional flow fields. Krylov techniques (Edwards et al. 1994) are quickly rising in popularity in analyzing fluid dynamical systems, and, with the size of computations steadily increasing, they should be expected to feature prominently in the stability analyses of complex flows. The general idea of Krylov iterative schemes is the formation of a lower-dimensional orthonormalized space $\mathbf{V}$ composed of snapshots of an evolving flow field, $\mathbf{V} \in \text{span}\{\mathbf{q}, \mathbf{Aq}, \mathbf{A}^2\mathbf{q}, \ldots, \mathbf{A}^{N-1}\mathbf{q}\}$, with each $\mathbf{A}^k\mathbf{q}$ obtained from a direct numerical simulation at a given time. Using orthogonal similarity transformations and proceeding from column to column in $\mathbf{V}$, one can reduce the matrix $\mathbf{A}$ to a $N \times N$ upper Hessenberg matrix $\mathbf{H}$ using the Arnoldi process. A projection of the flow dynamics, represented, for example, by the matrix exponential, onto this low-dimensional space will result in a significantly smaller system that can again be analyzed by direct methods,

$$\exp(\mathbf{A}t) \approx \mathbf{V}\exp(\mathbf{H}t)\mathbf{V}^H = \mathbf{VD}\exp(\mathbf{R}t)\mathbf{D}^{-1}\mathbf{V}^H =$$

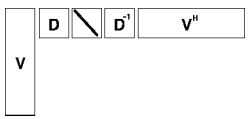

where $\mathbf{R}$ is a diagonal matrix of Ritz values and $\mathbf{D}$ containing the corresponding Ritz vectors. Each flow field $\mathbf{VD}$, expressed as a linear combination of orthonormalized

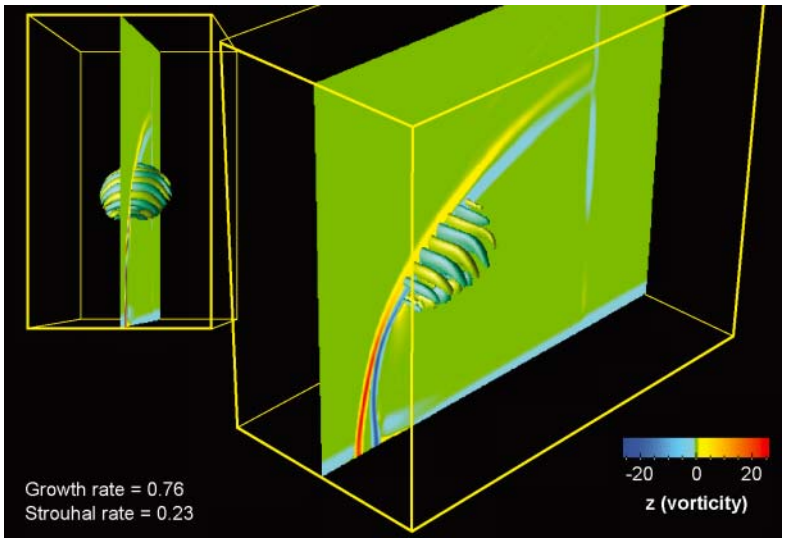

Figure 11

Three-dimensional visualization of the least stable global mode for a jet in cross flow. The global mode appears in the form of a localized wave packet at a location where a local Kelvin-Helmholtz instability is the strongest. The global modes have been determined from a direct numerical simulation via an iterative eigenvalue procedure.

fields from a direct numerical simulation, represents a global mode of the system. As an example, **Figure 11** shows the dominant global mode extracted from a direct numerical simulation of a jet in cross flow (Blossey & Schmid 2002). This least stable mode takes on the shape of a localized three-dimensional wave packet located on the upper shear layer where simulations and experiments report a strong Kelvin-Helmholtz-type instability.

The central message conveyed in this review is the importance of a multimodal viewpoint where the superposition of modal solutions can result in a markedly different disturbance behavior that could not be obtained by considering solely individual modes. Only the superposition of global modes can ensure that the relevant dynamics of the complex flow has been adequately captured and quantitatively described (Chomaz 2005). The shape and associated eigenvalues of the global modes may carry little information about the behavior of linear disturbances. An example of this phenomenon can be found in Schmid & Henningson (2002), where the characteristic timescale of an oscillating liquid sheet is given by the collective beating of global modes. The individual frequencies of the global modes have no relevance for the dynamics.

6. NONLINEAR EFFECTS: EXTENDING ADJOINTS

Any analysis based on the fundamental solution operator assumes that the governing equations are linear. Even though nonautonomous operators (such as the

time-dependent flows discussed in Section 3) can be treated, the description of nonlinear effects is out of reach of this technique. The framework based on a variational formulation of the stability problem, introduced above, however, can accommodate nonlinear governing equations.

To recapitulate, the formulation of stability calculations in the form of a variational principle consists of two parts: the cost functional that describes the quantity we wish to optimize (e.g., the growth of initial energy over a given time interval), and the constraints that are added using adjoint variables and that enforce the governing equations as well as initial conditions. No restrictions on the characteristics of the governing equations are given and the nonlinear Navier-Stokes equations could easily be enforced via an adjoint variable (Corbett 2000). However, some additional features arise when an iterative scheme is derived by setting the first variations of the Lagrangian to zero. Due to the nonlinear terms appearing in the Lagrangian, for example, $\int \tilde{u} v \frac{\partial u}{\partial y} dy$, a first variation with respect to δu will lead to the following term in the adjoint equation: $-\int \frac{\partial}{\partial y}(v\tilde{u})\delta u \, dy$, which demonstrates that the adjoint partial differential equation will be linear in the adjoint variables, but its coefficients will depend on the direct variables (in the above case, on v). This introduces additional complications for the numerical solution of the nonlinear optimization problem via an iterative scheme. During the forward sweep using the direct (nonlinear) equations, the flow fields have to be saved as they are needed (in reverse order) for the backward sweep using the (linear) adjoint equations (Zuccher et al. 2006). For long integration times and three-dimensional problems this can put significant strain on memory requirements and computational speed. Various techniques to improve these computational difficulties have been devised such as check pointing (Berggren 1998, Hinze et al. 2005) where only a few flow fields are stored during the forward sweep and interpolation is used to reconstruct flow fields for times in between the stored ones. An alternative technique uses sparsely time-staggered flow fields as initial conditions to advance the direct flow fields to the desired time. In any case, additional computational effort has to be exerted to extract stability information governed by nonlinear equations.

7. CONCLUSIONS, REMARKS, AND FUTURE DIRECTIONS

At the core of nonmodal stability theory lies the recognition that the linearized Navier-Stokes operator applied to most wall-bounded shear flows is nonnormal. As a consequence, the spectrum of the linearized equations reduces to an asymptotic tool describing only the long-term behavior of disturbances. More sophisticated approaches have to be taken, and more involved methods have to be employed, to accurately capture short-time behavior, which, in most cases, is more relevant to the overall flow physics. The matrix exponential (Equation 2.3) and resolvent (Equation 2.6b) (and their variants) are central to the analysis of nonmodal stability for deterministic problems, whereas the Lyapunov Equation 4.2 and the equation for the covariance matrix (Equation 4.6) probe the influence of stochastic effects on the evolution of linear perturbations. With minor modifications, these tools can address spatially varying flows or even nonlinear disturbances.

The exact location of eigenvalues is of little importance when characterizing the short-time behavior of nonnormal evolution processes. Moreover, it is often observed that eigenvalues of nonnormal operators are highly sensitive to perturbations, whereas the global behavior is not, thus lending additional support to the necessity for nonspectral analysis tools. The importance of inexact solutions, such as described by pseudospectra, resolvent norm contours, or pseudowave packets, expounds on the fact that "nearly solutions" (which are not necessarily near solutions) may be more relevant to the disturbance behavior than eigensolutions.

The approach outlined in this review, which describes stability characteristics based on the general response behavior of the linearized Navier-Stokes equations to initial conditions, external forcings, or internal perturbations (**Figure 1**), yields a rich and complete picture of disturbance behavior and paves the way for a more focused exploration of fluid processes in which instabilities are a crucial component. Admittedly, the introduced tools require a higher computational effort. However, the resulting wealth of information goes far beyond the dynamics of the least stable mode and more than justifies this effort.

Owing to ever increasing computational resources, direct numerical simulations of flows dominated by a wide range of scales and physical processes are now common. Large-scale simulations furnish an impressive amount of data, which is sometimes difficult to comprehend or analyze. Any systematic attempt at distilling the essential mechanisms and effective transport processes from these data should be welcomed and encouraged. It is reasonable to anticipate that direct numerical simulations will play an important role in hydrodynamic stability theory—not so much as a confirming tool but, rather, as a source of input data for a global mode decomposition. This decomposition will help in identifying dynamically relevant subregions (see **Figure 11**), while an appropriate superposition of the modes will capture the dominant perturbation dynamics.

Modern iterative schemes, such as Krylov subspace methods, will feature more prominently and will become as ubiquitous as the direct eigenvalue routines in current use. The symbiosis of direct numerical simulations (providing snapshots of disturbance dynamics), iterative techniques (extracting physically relevant bases), and nonmodal stability analysis (quantifying the dominant short-term disturbance behavior) will, in principle, enable the analysis of any flow amenable to a description by large-scale computations. Related fields, such as flow control and model reduction, will take the same direction.

The concept of stability is generally acknowledged to play a pivotal role in the transition from laminar to turbulent fluid motion; it has important technological consequences as air, marine, and automotive vehicles continue to push the limits of their operational envelope; in meteorology and environmental fluid dynamics, instabilities affect the formation of weather patterns or the efficiency of mixing processes—in short, due to the range of its applicability and the relevance of its predictions for many fluid transport processes, hydrodynamic stability theory will continue to occupy a central position within fluid dynamics research and be an integral part of many scientific inquiries. The tools of nonmodal stability theory are designed to help in this effort by correctly identifying preferred structures, detect important mechanisms, and

thus help gain the necessary insight and understanding that leads to a more targeted effort in the design and management of fluid dynamic processes.

ACKNOWLEDGMENTS

I wish to thank Dan Henningson and Nick Trefethen, who, long ago, got me interested in hydrodynamic stability and pseudospectra and generously supported me on my path over many years. I am also grateful to Patrick Huerre for welcoming me into LadHyX and for his kind support. I am indebted to Patrick Huerre, Nick Trefethen, Dan Henningson, Jörn Sesterhenn, and Christoph Mack for giving me many thoughtful comments that helped improve this review. The Alexander-von-Humboldt Foundation is warmly thanked for its generous and flexible support of part of this work. Finally, I wish to thank Donna Calhoun for useful hints regarding the visualization.

LITERATURE CITED

Alfredsson P, Matsubara M. 2000. Freestream turbulence, streaky structures and transition in boundary layer flows. *AIAA Pap. 2000–2534*

Aubry N. 1991. On the hidden beauty of the proper orthogonal decomposition. *Theor. Comput. Fluid Dyn.* 2:339–52

Bamieh B, Dahleh M. 2001. Energy amplification in channel flows with stochastic excitation. *Phys. Fluids* 13:3258–69

Bayly B. 1986. Three-dimensional instability of elliptical flow. *Phys. Rev. Lett.* 57:2160–63

Bender C, Orszag S. 1978. *Advanced Mathematical Methods for Scientists and Engineers*. New York: McGraw-Hill

Berggren M. 1998. Numerical solution of a flow-control problem: vorticity reduction by dynamic boundary action. *SIAM J. Sci. Comput.* 19:829–60

Berkooz G, Holmes P, Lumley J. 1993. The proper orthogonal decomposition in the analysis of turbulent flows. *Annu. Rev. Fluid Mech.* 25:539–75

Berlin S, Henningson D. 1999. A nonlinear mechanism for receptivity of freestream disturbances. *Phys. Fluids* 11:3749–60

Bertolotti F, Herbert T, Spalart P. 1992. Linear and nonlinear stability of the Blasius boundary layer. *J. Fluid Mech.* 242:441–74

Blossey P, Schmid P. 2002. Global stability analysis of a jet in cross flow. *Bull. Am. Phys. Soc.* 47(10):92

Boberg L, Brosa U. 1988. Onset of turbulence in a pipe. *Z. Naturforsch. Teil A* 43:697–726

Brandt L, Cossu C, Chomaz J-M, Huerre P, Henningson DS. 2003. On the convectively unstable nature of optimal streaks in boundary layers. *J. Fluid Mech.* 485:221–42

Briggs R. 1964. *Electron-Stream Interaction with Plasmas*. Cambridge, MA: MIT Press

Butler KM, Farrell BF. 1992. Three-dimensional optimal perturbations in viscous shear flows. *Phys. Fluids A* 4:1637–50

Chang C-L, Malik M. 1994. Oblique mode breakdown and secondary instability in supersonic boundary layers. *J. Fluid Mech.* 273:323–60

Chomaz J-M. 2005. Global instabilities in spatially developing flows: nonnormality and nonlinearity. *Annu. Rev. Fluid Mech.* 37:357–92

Choudhari M. 1993. Boundary layer receptivity due to distributed surface imperfections of a deterministic or random nature. *Theor. Comput. Fluid Dyn.* 4:101–17

Corbett P. 2000. *Nonmodal growth in boundary layers and its optimal control.* PhD thesis. École Polytech. Féd. Lausanne (EPFL), Lausanne, Switz.

Corbett P, Bottaro A. 2001. Optimal linear growth in swept boundary layers. *J. Fluid Mech.* 435:1–23

Crouch JD. 1994. Theoretical studies on the receptivity of boundary layers. *AIAA Pap. 94-2224*

Delbende I, Chomaz J-M, Huerre P. 1998. Absolute/convective instabilities in the Batchelor vortex: a numerical study of the linear impulse response. *J. Fluid Mech.* 355:229–54

Drazin P, Reid W. 1981. *Hydrodynamic Stability*. Cambridge, UK: Cambridge Univ. Press

Edwards W, Tuckerman L, Friesner R, Sorensen D. 1994. Krylov methods for the incompressible Navier-Stokes equations. *J. Comput. Phys.* 110:82–102

Farrell B, Ioannou P. 1993. Stochastic forcing of the linearized Navier-Stokes equations. *Phys. Fluids A* 5:2600–9

Farrell B, Ioannou P. 1996a. Generalized stability theory. Part I. Autonomous operators. *J. Atmos. Sci.* 53:2025–40

Farrell B, Ioannou P. 1996. Generalized stability theory. Part II. Nonautonomous operators. *J. Atmos. Sci.* 53:2040–53

Farrell B, Ioannou P. 2002. Optimal perturbation of uncertain systems. *Stochastics Dyn.* 2:395–402

Gallaire F, Ruith M, Meiburg E, Chomaz J-M, Huerre P. 2006. Spiral vortex breakdown as a global mode. *J. Fluid Mech.* 549:71–80

Gaster M. 1965. On the generation of spatially growing waves in the theory of hydrodynamic stability. *J. Fluid Mech.* 22:433–41

Gaster M, Grant T. 1975. An experimental investigation of the formation and development of a wave packet in a laminar boundary layer. *Proc. R. Soc. London Ser. A* 347:253–69

Goldstein ME, Hultgren LS. 1989. Boundary-layer receptivity to long-wave freestream disturbances. *Annu. Rev. Fluid Mech.* 21:137–66

Guégan A, Schmid P, Huerre P. 2006. Optimal energy growth and optimal control in swept Hiemenz flow. *J. Fluid Mech.* 566:11–45

Gustavsson H. 1991. Energy growth of three-dimensional disturbances in plane Poiseuille flow. *J. Fluid Mech.* 224:241–60

Herbert T. 1988. Secondary instability of boundary layers. *Annu. Rev. Fluid Mech.* 20:487–526

Hill D. 1995. Adjoint systems and their role in the receptivity problem for boundary layers. *J. Fluid Mech.* 292:183–204

Hinze M, Walther A, Sternberg J. 2005. An optimal memory-reduced procedure for calculating adjoints of the instationary Navier-Stokes equations. *Optim. Control Appl. Methods* 27:19–40

Hœpffner J. 2006. *Stability and control of shear flows subject to stochastic excitations.* PhD thesis. R. Inst. Tech. (KTH), Stockholm, Swed.
Horn RA, Johnson CR. 1991. *Topics in Matrix Analysis*. Cambridge, UK: Cambridge Univ. Press
Huerre P, Monkewitz PA. 1990. Local and global instabilities of spatially developing flows. *Annu. Rev. Fluid Mech.* 22:473–537
Iserles A, Marthinsen A, Nørsett S. 1999. On the implementation of the method of Magnus series for linear differential equations. *BIT Numer. Math.* 39:281–304
Jacobs R, Durbin P. 2001. Simulations of bypass transition. *J. Fluid Mech.* 428:185–212
Joseph D. 1976. *Stability of Fluid Motions I*. New York: Springer-Verlag
Jovanović MR, Bamieh B. 2001. The spatio-temporal impulse response to the linearized Navier-Stokes equations. In *Proc. 2001 Am. Control Conf., Arlington, VA*, pp. 1948–53
Jovanović MR, Bamieh B. 2005. Componentwise energy amplification in channel flows. *J. Fluid Mech.* 543:145–83
Juarez LH, Ramos E. 2003. Direct numerical simulation of transition to turbulence in an oscillatory channel flow. *C.R. Méc.* 331:55–60
Khalil H. 2002. *Nonlinear Systems.* Englewood Cliffs, NJ: Prentice Hall
Klebanoff P, Tidstrom K, Sargent L. 1962. The three-dimensional nature of boundary layer instability. *J. Fluid Mech.* 12:1–34
Le Gal P, Croquette V. 2000. Visualization of the space-time impulse response of the subcritical wake of a cylinder. *Phys. Rev. E* 62:4424–26
Liu J. 2003. *A First Course in the Qualitative Theory of Differential Equations*. Englewood Cliffs, NJ: Prentice Hall
Luchini P, Bottaro A. 2001. Linear stability and receptivity analysis of the Stokes layer produced by an impulsively started plate. *Phys. Fluids* 13:1668–78
Mack LM. 1963. The inviscid stability of the compressible laminar boundary layer. *Space Progr. Summ. No. 37-23* p. 297, Jet Propuls. Lab., Pasadena, CA
Morkovin MV. 1960. On the many faces of transition. In *Viscous Drag Reduction*, ed. CS Wells, pp.1–31. New York: Plenum
Nocedal J, Wright SJ. 2000. *Numerical Optimization.* New York: Springer-Verlag
Obremski H, Fejer A. 1967. Transition in oscillating boundary layer flow. *J. Fluid Mech.* 29:93–111
Orr WMcF. 1907. The stability or instability of the steady motions of a perfect liquid and of a viscous liquid. *Proc. R. Irish Acad. A* 27:9–138
Orszag SA. 1971. Accurate solution of the Orr-Sommerfeld stability equation. *J. Fluid Mech.* 50:689–703
Orszag SA, Patera AT. 1983. Secondary instability of wall-bounded shear flows. *J. Fluid Mech.* 128:347–85
Pierrehumbert RT. 1986. Universal short-wave instability of two-dimensional eddies in an inviscid fluid. *Phys. Rev. Lett.* 57:2157–60
Pralits JO, Airiau C, Hanifi A, Henningson DS. 2000. Sensitivity analysis using adjoint parabolized stability equations for compressible flows. *Flow Turbul. Combust.* 65:321–46

Ravier S, Abid M, Amielh M, Anselmet F. 2006. Direct numerical simulations of variable-density plane jets. *J. Fluid Mech.* 546:153–91
Reddy SC, Henningson DS. 1993. Energy growth in viscous channel flows. *J. Fluid Mech.* 252:209–38
Reddy SC, Schmid PJ, Henningson DS. 1993. Pseudospectra of the Orr-Sommerfeld operator. *SIAM J. Appl. Math.* 53:15–47
Reynolds O. 1883. An experimental investigation of the circumstances which determine whether the motion of water shall be direct or sinuous, and the law of resistance in parallel channels. *Philos. Trans. R. Soc. London Ser. A* 173:935
Riley J, Gad-el Hak M. 1985. The dynamics of turbulent spots. In *Frontiers in Fluid Dynamics*, ed. SH Davis, JL Lumley, pp. 123–55. Berlin: Springer-Verlag
Schlichting H. 1933. Berechnung der Anfachung kleiner Störungen bei der Plattenströmung. *ZAMM* 13:171–74
Schmid PJ, Henningson DS. 2001. *Stability and Transition in Shear Flows*. New York: Springer-Verlag
Schmid PJ, Henningson DS. 2002. On the stability of a falling liquid curtain. *J. Fluid Mech.* 463:163–71
Schmid PJ, Henningson DS, Khorrami M, Malik M. 1993. A sensitivity study of hydrodynamic stability operators. *Theor. Comput. Fluid Dyn.* 4:227–40
Schmid PJ, Kytömaa HK. 1994. Transient and asymptotic stability of granular shear flows. *J. Fluid Mech.* 264:255–75
Sirovich L. 1987. Turbulence and the dynamics of coherent structures. Part I-III: *Q. Appl. Math.* 45:561–82
Skogestad S, Postlethwaite I. 1996. *Multivariable Feedback Control - Analysis and Design*. New York: Wiley
Sommerfeld A. 1908. Ein Beitrag zur hydrodynamischen Erklärung der turbulenten Flüssigkeitsbewegungen. In *Proc. 4th Int. Congr. Math., Rome* pp. 116–24
Taylor G. 1923. Stability of a viscous fluid contained between two rotating cylinders. *Philos. Trans. R. Soc. London Ser. A* 223:289–343
Theofilis V. 2003. Advances in global linear instability analysis of nonparallel and three-dimensional flows. *Prog. Aerosp. Sci.* 39:249–315
Tollmien W. 1929. Über die Entstehung der Turbulenz. *Nachr. Ges. Wiss. Göttingen* pp. 21–44
Trefethen L. 1997. Pseudospectra of linear operators. *SIAM Rev.* 39:383–406
Trefethen L, Embree M. 2005. *Spectra and Pseudospectra: The Behavior of Nonnormal Matrices and Operators.* Princeton: Princeton Univ. Press
Trefethen L, Trefethen A, Reddy S, Driscoll T. 1993. Hydrodynamic stability without eigenvalues. *Science* 261:578–84
Verhulst F. 2006. *Nonlinear Differential Equations and Dynamical Systems*. Berlin: Springer-Verlag
Zhou K, Doyle J, Glover K. 1996. *Robust and Optimal Control*. Englewood Cliffs, NJ: Prentice Hall
Zuccher S, Bottaro A, Luchini P. 2006. Algebraic growth in a Blasius boundary layer: Nonlinear optimal disturbances. *Eur. J. Mech. B* 25:1–17

Annual Review of
Fluid Mechanics

Volume 39, 2007

Contents

Indexes

Errata

An online log of corrections to *Annual Review of Fluid Mechanics* chapters (1997 to the present) may be found at http://fluid.annualreviews.org/errata.shtml